Computer Simulation of Interfacial Zone Microstructure and Its Effect on the Properties of Cement-Based Composites

DALE P. BENTZ, ERIK SCHLANGEN,* and EDWARD J. GARBOCZI, Building and Fire Research Laboratory, National Institute of Standards and Technology

... imagination is the tool which has to be used if the impossible is to be accomplished.

--Leo Szilard

Much recent research on the materials science of concrete has focused on the characteristics of the interfacial zone between cement paste and aggregate and its effects on mechanical and other properties. This chapter reviews recent computer modeling work on these topics, including the formation mechanisms of interfacial zone microstructure, the effects of cement paste and aggregate physical properties on this microstructure, the percolation of individual interfacial zones as a function of aggregate size distribution and content, and the mechanical and transport properties of cement paste-aggregate composites. Model results are compared with experimental results from the available literature.

Introduction

The properties, and thereby performance, of cement-based materials are to a large degree a function of their microstructure. Understanding the relationships between microstructure and properties is critical to the design and improvement of systems and structures. For concrete, elucidating these relationships is complicated by the composite nature of the material. Thus,

*Permanent address: Delft University of Technology, Stevin Laboratory, The Netherlands.

Materials Science of Concrete IV, J.P. Skalny and S. Mindell, Editors, American Ceramic Society, Westerville, OH, 1995

studying cement paste microstructure is informative but not sufficient in trying to understand concrete performance. To truly understand this complex material, its composite nature must be studied; this means studying the properties of its components (mainly hydrated cement paste and inclusions such as aggregate and reinforcing steel) and the interfaces that exist between them. Research on the role of these interfacial zones (IZs) in concrete performance has increased rapidly in the past few years as witnessed by a recent conference devoted entirely to this subject.[1] Also, excellent summaries of IZ research can be found in a number of review articles that have appeared over the last decade or so.[2–4] The IZ may be of particular importance in high-quality composites such as high-strength concrete and fiber-reinforced cement-based materials.[5]

Research efforts on interfacial zones have concentrated on answering a variety of questions, such as: What are the characteristic microstructural features of the IZ in concrete? What are the mechanisms that lead to the formation of these IZs? How can the IZ microstructure be modified and improved? To what extent, if any, does the IZ microstructure affect the mechanical and transport properties of concrete? Whereas these questions have all been approached to some degree from an experimental standpoint, this chapter will focus on the use of computer modeling techniques to study the nature of the IZ in concrete.

The models reviewed in this chapter can all be classified as fundamental models,[6] because they directly handle the microstructural features that determine the property being computed. They can be further classified by the length scale at which they operate. For example, a micrometer-scale model ignores the nanometer-scale pore structure of the calcium-silicate-hydrate gel product, but attempts to directly represent the capillary pore space. A millimeter-scale model treats cement paste as a continuum material, and the interfacial zone as a monophase, very thin continuous region. It would be very useful to have a model that covers all the relevant length scales simultaneously. However, as concrete contains length scales of importance from nanometers to centimeters, covering a size range of seven orders of magnitude,[7] it is currently impossible, even with present-day supercomputers, to handle all of the range with one model. Rather, an approach is taken where a given model operates at a given length scale, and then passes its results upward to a model operating at higher length scales. This approach will be illustrated in this review, although all the pieces have not been put together for all the topics that will be discussed.

Discussion of the two areas to be covered, interfacial zone microstructure and its effect on concrete properties, is arranged in the following manner. The first topic to be discussed is how the microstructure of a single interfacial zone has been modeled at the micrometer level. It is then shown how this information is fed in to a higher-order model that studies the effects on microstructure of many thousands of interfacial zones together in a mortar or concrete. Then the modeling of the linear elastic properties of cement paste at the micrometer hardware field, this situation will probably change dramatically in just a few years.

The starting image for the cement paste hydration model consists of a representation of the cement particles dispersed in water. In two dimensions, this image could consist of model circular cement particles or an actual image of cement particles separated into their component phases using scanning electron microscopy (SEM) and image analysis techniques.[9] Figure 1 (p. 186) shows a color-coded image of a Type-I portland cement that has been segmented into six phases: tricalcium silicate (C_3S), dicalcium silicate (C_2S), tricalcium aluminate (C_3A), tetracalcium aluminoferrite (C_4AF), gypsum, and black (water-filled) porosity. In three dimensions, cement particles have generally been represented by digitized spheres but could perhaps be based on actual three-dimensional image sets obtained from serial sectioning[10] or microtomographic techniques.[11,12] A single aggregate can be represented by a flat plate, as shown in Fig. 1, or by a simple geometrical shape like a cube, which must be much larger than the individual cement particles to reflect actual aggregate size relative to cement particles.

The next step in modeling microstructure development during hydration is to specify a set of rules, consisting of chemical reactions and "physical" mechanisms, to simulate the hydration process. Because the starting microstructure is digital-image based, a set of cellular automata-type rules may be specified to control which event occurs at each pixel during each step of the model hydration.[13] Figure 2 illustrates the rules constituting the current version of the NIST cement microstructure model. The rules have been selected to follow the overall observed mechanisms of cement hydration without adhering strictly to the fine details. The underlying chemical reactions and their volume stoichiometries are provided in Ref. 13 and are based on generally accepted phase stoichiometries taken from the literature.[14–16]

The rules are implemented in a series of dissolution/diffusion/reaction cycles as illustrated in the sequence shown in Fig. 3 (p. 187). Material is dissolved randomly from the cement particle surfaces in contact with the pore space, creating diffusing species as indicated in Fig. 2. The second portion of Fig. 3 shows the point in the model where all of the cement particle surfaces in contact with pore space have been identified and highlighted in white, whereas the central portion shows the model after generation of the diffusing species. Each diffusing species undergoes random walk diffusion within the pixels constituting the pore space until a reaction occurs according to the rules depicted in Fig. 2. When all diffusing species generated by a given dissolution have reacted, the cycle is complete and a new dissolution can be performed. By keeping track of the phases present at the end of each cycle, the degree of hydration and heat generated by the reactions[9] can be determined as a function of the number of cycles.

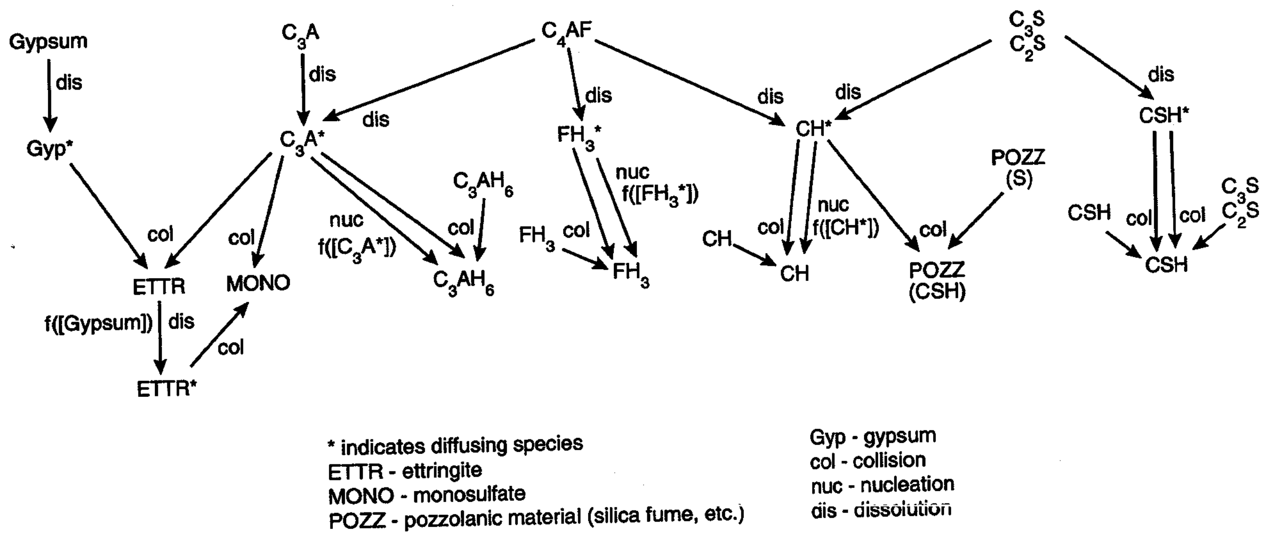

Fig. 2 Diagram of rules constituting the NIST cement microstructure development model. (Reprinted with permission from Ref. 13.)

For instance, the fourth and fifth portions of Fig. 3 show the results predicted by the model after 32 and 76% of the initial cement, respectively, has hydrated.

When a single aggregate is present in the computer model microstructure, its effects on microstructure may be quantified by measuring the phase fractions present as a function of distance from the aggregate. Scrivener[17,18] has pioneered a technique for making similar measurements on real specimens using SEM and image analysis techniques.

Finally, it is of interest to extend results for a single IZ to a system containing thousands of aggregates. Due to resolution limitations, digital-image-based techniques are not as appropriate for this problem. Here, a continuum hard-core/soft-shell computer model[19] has been used to study the percolation or connectivity of IZ in mortar and concrete.[20] The basic building block of this model is a particle with an inpenetrable hard core surrounded by a concentric penetrable soft shell. For concrete, the hard cores would represent the aggregates since they cannot overlap one another, while the soft shells would be representative of the IZ, since they are free to overlap one another and other aggregates. The hard-core aggregates are randomly placed, from largest to smallest, in a three-dimensional box using periodic boundaries. A constant-thickness IZ (soft shell) is then added to each hard core. The periodic boundaries require that if a portion of a particle extends beyond one or more faces of the box, it is completed on the opposite side(s) of the box. For a given IZ thickness, aggregate volume fraction, and aggregate size distribution, one is interested in whether the IZ around each aggregate will link up to form a connected pathway ("short circuit") across the sample. Percolation could have significant effects on strength and durability since the IZs are generally inferior to the bulk paste with respect to these properties. Computational techniques have been developed to determine this IZ percolation for systems containing up to 500 000 aggregates (equivalent to about 27 000 mm^3 of concrete).[20]

Formation Mechanisms and General Microstructural Features

Since the IZ was first observed in 1956 by Farran,[21] many researchers have studied its characteristics. Studies have been performed both on ideal "flat" surface single aggregates[22–24] and actual mortar and concrete specimens.[17,18,25,26] The characteristics of the aggregate-cement paste IZ have been observed to exist also at steel rebar-cement paste interfaces.[27,28] The generally accepted view of the IZ in ordinary portland cement concrete is that it consists of a region up to 50 μm wide surrounding each aggregate where the volume fractions of the phases constituting the microstructure are significantly different from those in the bulk paste. In this region, there is less unhydrated cement and higher porosity, with generally larger pores than those found in the bulk paste. Additionally, large oriented crystals of calcium hydroxide are often observed in the IZ regions[29] along with a greater concentration of ettringite, while less of the calcium-silicate-hydrate gel product forms in the IZ than in the bulk paste.[3,30] Figure 4 shows a plot of phase volume fractions as a function of distance from the aggregate surface for a 63% hydrated, 0.45 water/cement ratio, simulated microstructure such as the one shown in Fig. 1. The values in Fig. 4 are based on averaging the results for five separate configurations of initial microstructures like the one shown in Fig. 1. The results in Fig. 4 agree well with the general observations mentioned above.

The initial modeling efforts at NIST investigated the mechanisms of IZ development in ordinary portland cement concrete.[6,31] The simulations were performed on two-dimensional microstructures containing a single square aggregate. Two major mechanisms were identified as contributing to the development of the IZ. The first, denoted the "wall effect," comes about because of packing constraints. Since the aggregate is large relative to the cement particles, it acts as a relatively smooth wall for them. The presence of the wall causes less-efficient arrangement of the nearby cement, resulting in fewer cement particles being present near the aggregate surface than in the bulk paste far away from an aggregate.[18] Bleeding, if present, would further intensify this effect by producing a layer of water at the aggregate surface. Even without significant bleeding, however, there will be a deficiency of cement near the aggregate surface in the fresh concrete mix due to the wall effect. A secondary mechanism identi-

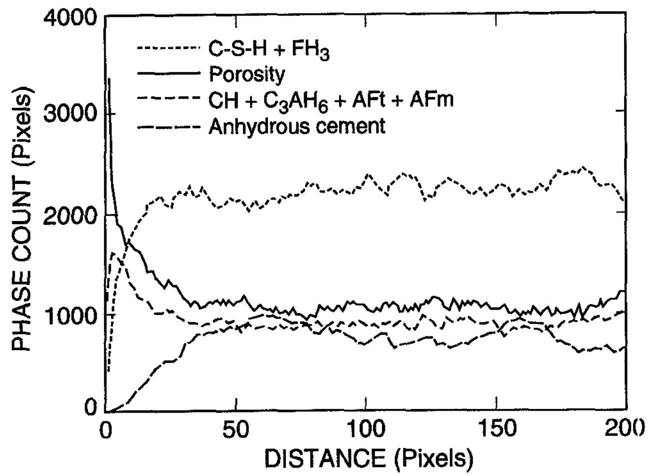

Fig. 4. Phase counts vs distance from aggregate surface, water/cement ratio = 0.45, 63% hydration. (Reprinted from Ref. 9.)

fied in the intial computer simulation study[31] was the one-sided growth effect. As hydration occurs in regions far from an aggregate surface, the pore volume is being filled with hydration products from all directions, on average. For a point near an aggregate, however, reactive growth only occurs from the paste side. This effect is minor when compared to the wall effect, but is still significant in increasing the porosity of the IZ relative to the bulk paste very near to the aggregate. Recently, a similar computer simulation approach has been utilized to qualitatively study the effects of mixing and flocculation on the initial distribution of cement particles near an aggregate surface.[32]

In addition to phase fractions, several researchers have used electron probe microanalysis to study the molar ratio of Ca to Si in the IZ region.[24,33,34] In the computer model, this ratio can be conveniently determined based on the measured volumetric phase fractions and the molar volumes of the individual phases. Figure 5 shows a plot of Ca/Si for a 0.45 water/cement ratio computer model C_3S paste after 77% hydration. The Ca/Si ratio is seen to settle to its expected bulk value of 3 (for pure C_3S) at a distance roughly corresponding to the average cement particle size used in the initial mix (16 pixels). Approaching the interface, this ratio increases monotonically to a maximum value slightly larger than 5, which is in excellent agreement with the experimental observations of Larbi and Bijen,[33] who observed a maximum value of about 5 for a 28-day-old Type I portland cement paste with a water/cement ratio of 0.40, and Yuan and

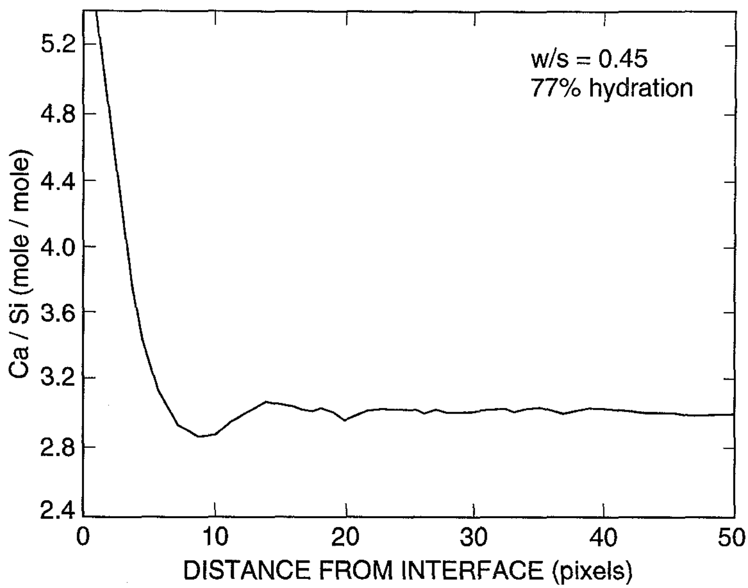

Fig. 5. Ca/Si ratio vs distance from aggregate surface for C_3S paste with water/cement ratio = 0.45 after 77% hydration. (Adapted from Ref. 44.).

Odler,[24] who measured a maximum value of about 6 for a hydrated pure C_3S paste with a water/cement ratio of 0.38. Since, initially, this value would be constant everywhere, the results support the hypothesis that calcium ions are diffusing into the IZ regions at a much faster rate than are silicate ions.[3,35]

Effects of Cement Paste Characteristics on IZ Microstructure

One advantage of computer models is that a large number of parameters can be varied in a shorter amount of time than that required for a comparable experimental program. Thus, once a model has been validated against experiments, it may be efficiently used to study a wide variety of system configurations. The NIST microstructure models have been used to study the effects of cement particle size, mineral admixture size, and reactivity on IZ microstructure.[36]

To study particle-size effects in as accurate a manner as possible, a continuum spherical particle packing program (basically the hard-core/soft-shell program described in the "Computational Techniques" section with a soft-shell thickness of zero) has been used. Here, the cement particles are selected from a size distribution obtained from a sieve analysis and placed into a three-dimensional box 200 μm on a side. Rigid walls are present on two sides of the sample box to represent aggregates while periodic boundaries are maintained on the other four sides. Systematic point sampling[37] is used to quantify the initial cement and porosity (water) volume fractions as a function of distance from the aggregate surfaces. Using sieve size distributions presented by van Breugel,[38] results are shown in Fig. 6 for two cements at various water/cement ratios.

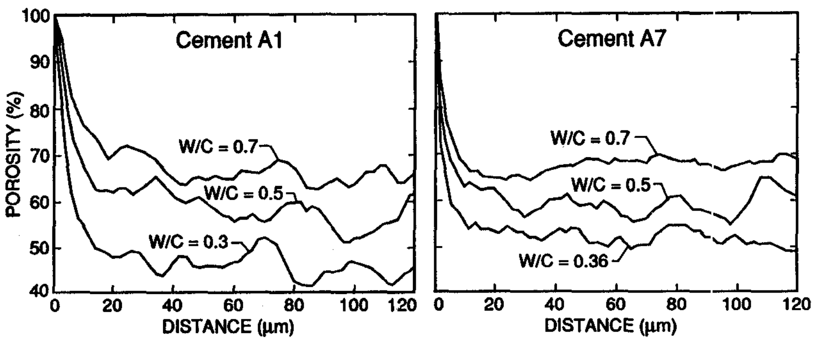

Fig. 6. Porosity fraction near aggregate before any hydration. (Reprinted from Ref. 36.)

Cement A1 has a median particle size, on a mass basis, of about 28 μm, whereas the median particle size of cement A7 is about 11 μm. For both cements, the thicknesses of the initial IZ (before any hydration), as denoted by the distance at which the porosity first approaches its "average" value, correspond closely to their median particle diameters. Conversely, water/cement ratio has little effect on the initial IZ thickness, although it significantly affects the gradient in porosity as the aggregate surface is approached.

The NIST microstructure models have also been applied to studying the effects of mineral admixtures on the IZ.[39] Once again, an aggregate is first centered in the computational volume of material, followed by the addition of the cement (in this case, pure C_3S) and mineral admixture particles in order of largest to smallest. Here, a percentage of the cement on a mass basis is replaced with a mineral admixture of a specific size (distribution) and pozzolanic activity, while maintaining a constant water/solids ratio. The pozzolanic activity specifies how many volume units of calcium hydroxide can be consumed in reacting with one volume unit of the mineral admixture to form pozzolanic-derived C-S-H gel. For instance, silica fume has been modeled as small 1-pixel (1-μm) particles assumed to consist of 100% SiO_2. Larger particles may be used to model agglomerated silica fume or fly ash. Additionally, fly ash is usually assigned a lower pozzolanic activity since it is typically about 50% SiO_2 and generally less efficient in consuming calcium hydroxide than silica fume is.[40]

Figure 7 (p. 188) shows the IZ microstructures, after 77% hydration, for a variety of cement-mineral admixture pastes. The two-dimensional images shown in Fig. 7 were taken just above the surface of a three-dimensional cubic aggregate 100^3 pixels in size centered in a sample box 200 pixels on a side. The addition of the mineral admixtures significantly affects the IZ microstructure. For instance, the system containing 20% small silica fume particles has a much denser and more homogeneous appearance than the plain cement paste system, in agreement with a number of experimental observations of the effects of silica fume on IZ microstructure.[41–44] However, if the silica fume is not well dispersed and tends to agglomerate into larger clumps within the paste, its effectiveness is reduced as seen in Fig. 7. The reason for this is shown more clearly in Fig. 8, which contrasts the initial particle configurations for microstructures containing small well-dispersed and larger (clumped) mineral admixture particles. Here, the ability of the smaller particles to fill in a fraction of the high-porosity region near the aggregate surface is clearly seen. Additionally, in the case of silica fume, these small particles in the IZ will react with the high flux of calcium ions diffusing into the IZ region during hydration to form pozzolanic-derived C-S-H, resulting in a denser IZ and a more homogeneous overall microstructure. This homogeneity is exemplified by the Ca/Si ratio, which, in contrast to the graph in Fig. 5, remains nearly constant as the aggregate is approached.[44]

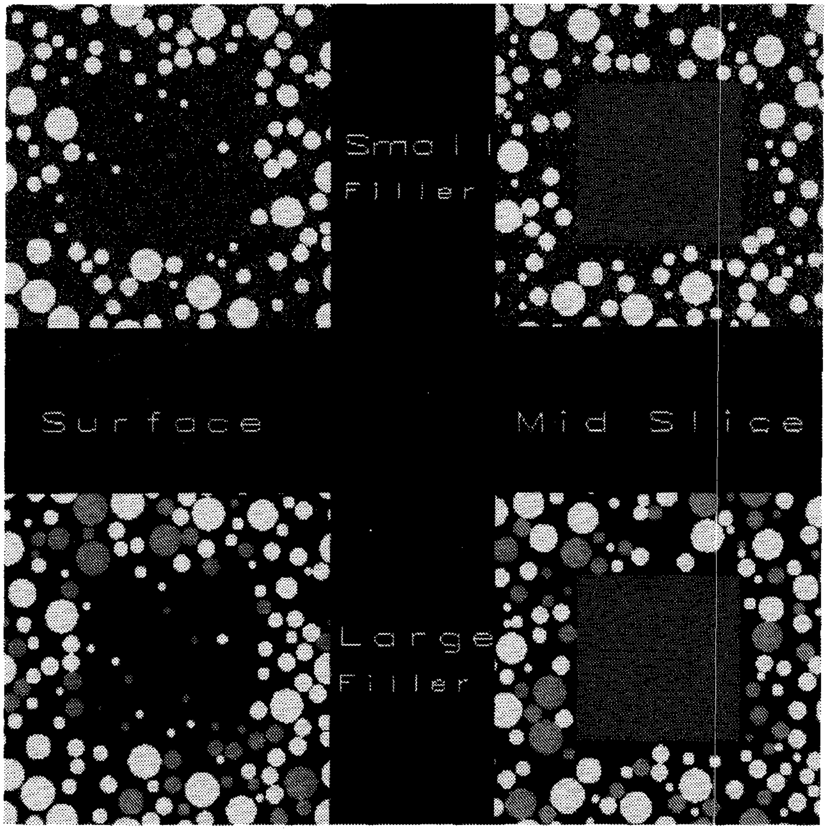

Fig. 8. Initial particle packings for C_3S (white) paste containing 20% small and large mineral admixture particles (light gray) with water/solid ratio = 0.45, around aggregate (dark gray). (Reprinted from Ref. 39.)

As mentioned previously, the IZ microstructure can be quantified by measuring the volumetric phase fractions as a function of distance from the aggregate surface. Figure 9 provides a plot of the cement + C-S-H phase fraction for each of the systems shown in Fig. 7. The cement and C-S-H have been combined based on the assumption that these two phases are the main contributors to the strength of the matrix phase of a cement-based material. In this plot, the small silica fume particles are seen to raise this phase fraction in the bulk paste (due to the pozzolanic reaction between CH and silica fume) and to also sharply reduce the reduction in this value as the aggregate surface is approached. Fly ash is seen to be less beneficial than silica fume in this respect,

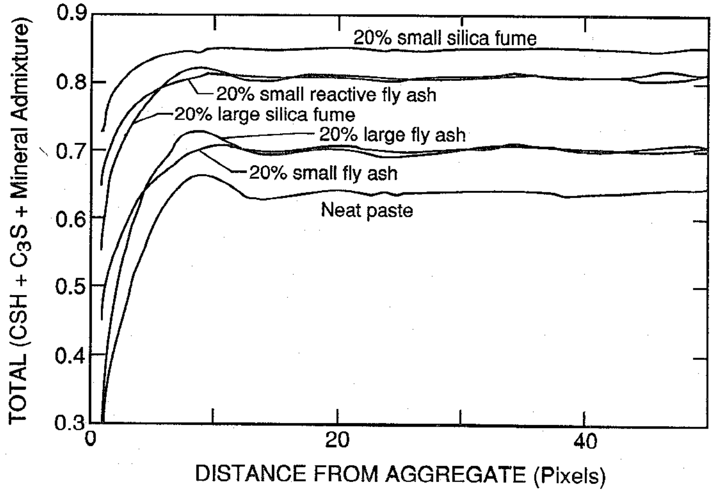

Fig. 9. Plot of total C-S-H + C_3S + mineral admixture fraction as a function of distance from aggregate surface for plain and admixture-modified C_3S pastes with water/solid ratio = 0.45 at 77% hydration. (Reprinted from Ref. 39.)

due to both its larger size and lower pozzolanic activity. However, the system based on very fine (1-μm) fly ash particles assigned a pozzolanic activity half that of silica fume offers comparable performance to the agglomerated silica fume system. Many experimental studies have shown that the finest portions of a fly ash are indeed the most effective in improving the properties of the fresh concrete and the strength of the hardened material.[45–48]

Effects of Aggregate Characteristics on IZ Microstructure

The NIST microstructure models can also be used to study the effects of aggregate characteristics on IZ microstructure. The two major properties studied to date have been absorptivity and reactivity.

Several researchers have noted that the IZ in lightweight concrete is denser than that in ordinary concrete and may be, in fact, even denser than the bulk paste microstructure.[49,50] Fagerlund has suggested that the lightweight aggregate particles may act as filters, drawing in water and pulling cement particles toward their surfaces.[51] To investigate the effects of this filtration effect on hydrated microstructures, the microstructure model is used, but the initial dispersion of cement particles is modified by moving all cement particles a fixed distance (number of pixels) toward the aggregate surface, as shown in Fig. 10, to simulate

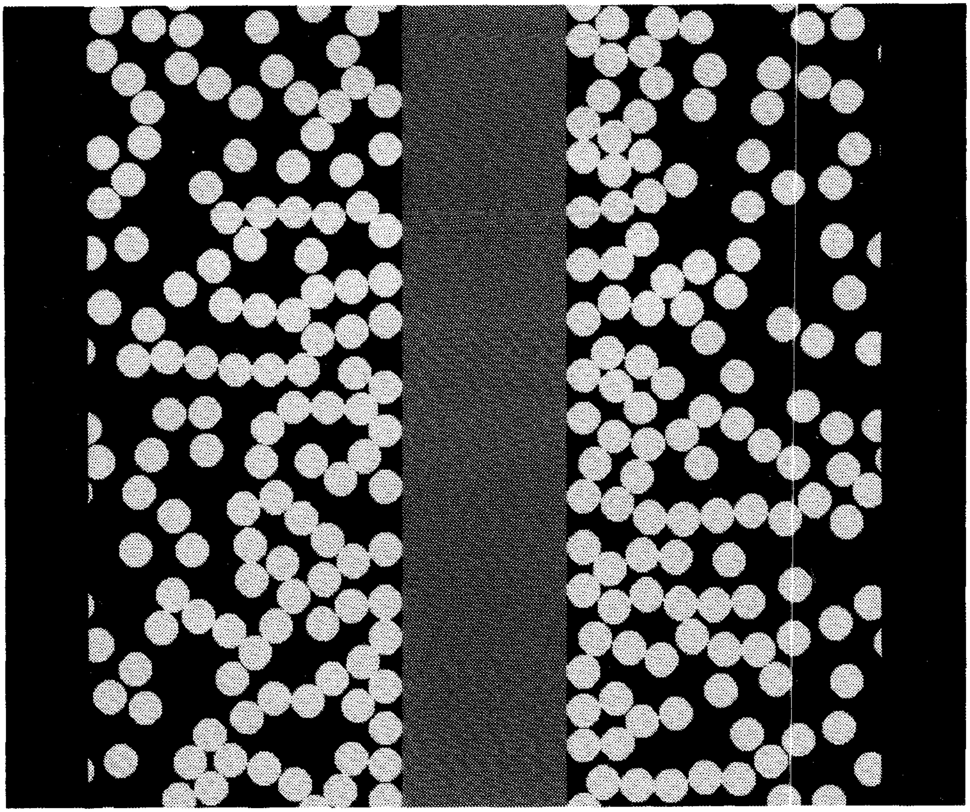

Fig. 10. Initial microstructure of C_3S grains (white) (after absorption) for an absorptive aggregate (gray). (Reprinted from Ref. 36.)

absorption by the aggregate. This results in an increase in cement volume fraction near the aggregate surface, somewhat offsetting the wall effect. The phase fractions after hydration are shown in Fig. 11, which contrasts a lightweight absorptive aggregate with a normal-weight aggregate, both with a paste water/cement ratio of 0.39 and a degree of hydration of 77%.[36] The plots of porosity and C_3S + C-S-H both exhibit improvement for the absorptive aggregate system, implying a denser IZ. The one-sided growth effect will still be operative so that within 5–10 pixels of the aggregate, the porosity will increase and the C_3S + C-S-H will decrease but not nearly as substantially as for the normal-weight concrete. In addition, in real concrete the roughness of the light-

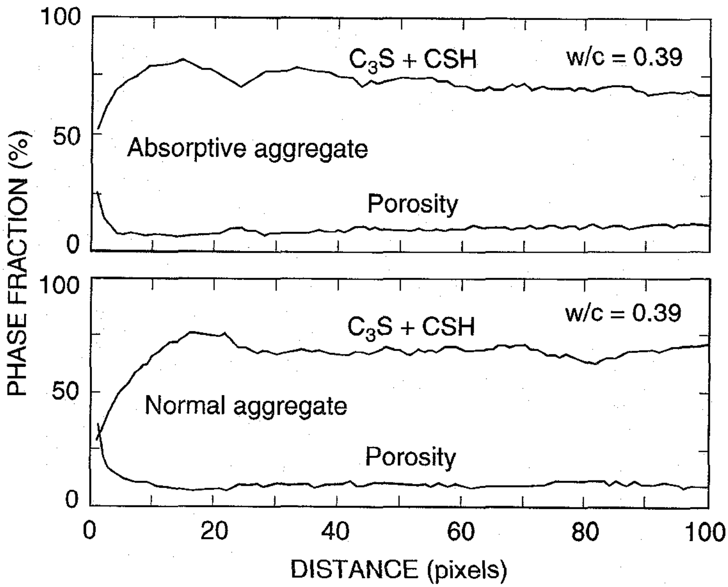

Fig. 11. Quantitative phase analysis for absorptive aggregate microstructure after 77% hydration. (Adapted from Ref. 36.)

weight aggregate may play a role. In addition to providing mechanical interlocking, the roughness may allow the irregular cement particles to be drawn tightly against the rough aggregate surface in a "lock-and-key" fashion to further eliminate the wall effect.[36]

Another scenario that has been investigated using the NIST microstructure model is the case of a reactive aggregate. Berger has prepared concrete mixes using cement clinker as aggregate and attributed the increased strengths of these systems to an improved aggregate-cement paste bond.[52] Obviously, a reactive aggregate will offset the one-sided growth effect as the aggregate too will contribute to product formation in the IZ paste. Cement clinker has the additional advantage that it is generally somewhat porous, so it may absorb some water from the cement paste, leading to the benefits described above for the absorptive aggregate. To model a reactive aggregate, the aggregate is assigned the same phase identifier as the cement particles so that it too may dissolve and undergo the hydration reactions. Because of its small surface-to-volume ratio, however, only a thin surface layer will undergo substantial hydration. Figure 12 (p. 189) shows the hydrated microstructure for a reactive absorptive aggregate, and Fig. 13 provides plots of porosity and C_3S + C-S-H vs distance from the

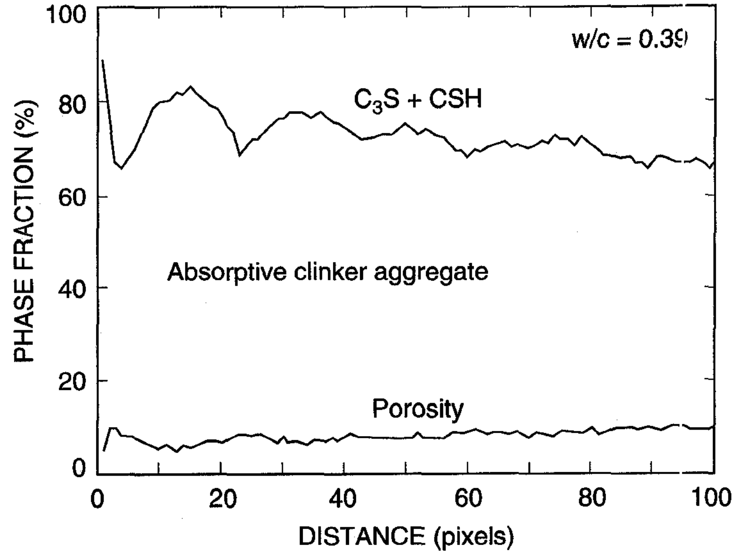

Fig. 13. Quantitative phase analysis for absorptive clinker aggregate microstructure after 75% hydration. (Adapted from Ref. 36.)

(initial) aggregate surface.[36] Here, it is clearly observed that these phases are now nearly homogeneous throughout the microstructure, with actually some increase in the C_3S + C-S-H phase as the aggregate surface is approached. The reactive absorptive aggregate addresses both the wall and one-sided growth effects, resulting in a more uniform IZ microstructure. Although using cement clinkers as aggregates may be prohibitive, since only a surface layer reacts substantially, similar performance should be obtainable using an inert aggregate with a reactive surface layer. Recent experimental studies have definitively demonstrated the feasibility of using a surface layer approach to enhance cement-aggregate IZ microstructure and improve concrete performance.[53–56]

Percolation of Interfacial Zones in Mortar and Concrete

To even attempt to model the effects of IZ microstructure on the bulk properties of a composite, it is necessary to extend the studies of a single IZ to consider the case present in mortar or concrete, where thousands of interfacial zones are present even in samples as small as 1000 mm^3. It is then essential to first determine the connectivity of the interfacial zones, since this will control their effect on bulk properties. If the individual IZs interconnect to percolate across a specimen, the bulk properties of the specimen would be expected to change, since pathways of larger pores will then be available for faster fluid or ion transport.

Using mercury intrusion porosimetry, Winslow and Lui[57] have shown that the pore structure of cement paste in concrete and mortar is quite different from that of plain cement paste. The main difference is that a substantial fraction of pores are larger than the threshold intrusion diameter for the plain cement paste matrix. The threshold intrusion diameter is defined by the pressure at which the mercury becomes continuous across the sample. Its experimental signature is an inflection point in the intrusion curve.[58] From microscopy, as was discussed in earlier sections, it is known that IZ pores exist that are significantly larger than ordinary cement paste pores. For these larger pores to be detected in the mercury intrusion experiment, at their proper diameter, implies that the individual IZs would have to percolate across the specimen. Otherwise, these larger pores could be reached by the mercury only through smaller, interconnected bulk cement paste pores, and their volume would consequently be assigned to these smaller bulk paste pores.

IZ percolation can be modeled using the hard-core/soft-shell model outlined in the "Computational Techniques" section. A computer simulation study has been conducted in conjunction with an experimental program for a series of mortars of increasing sand content.[20] Figure 14 shows the pore-size distributions for the mortars all at a water/cement ratio of 0.4. All curves have been normal-

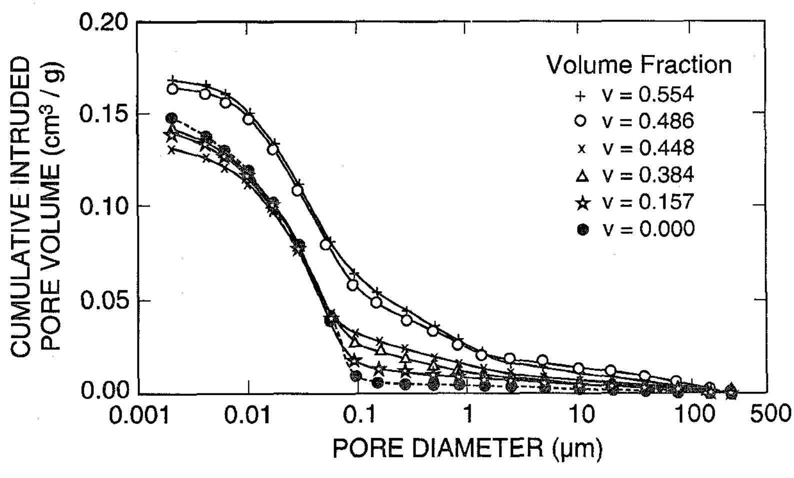

Fig. 14. Mercury intrusion porosimetry for mortars with varying sand contents. (Reprinted with permission from Ref. 20.)

ized to indicate intruded pore volume per gram of cement paste. As the sand content is increased, an increase in the coarse (>0.1 μm) pores is observed. Furthermore, when the sand content is increased from 44.8 to 48.6 vol%, a sharp increase in the coarse porosity occurs. Further increases in sand content have little effect on the cumulative intruded pore volume curve. Similar experimental results have been obtained by Feldman[59] at a water/cement ratio of 0.6. The dramatic increase in detectable coarse porosity as the sand content is increased from 44.8 to 48.6% suggests a percolation phenomena.

The hard-core/soft-shell model was used to model the experimental mortar systems by using the same sand (hard-core) size distribution and varying the IZ (soft-shell) thickness and sand content. For each IZ thickness and sand content, the fraction of the IZ regions that were percolated across a cubic specimen 10 mm on a side was determined. Figure 15 shows a plot of the fraction of IZ connected vs sand content for IZ thicknesses ranging from 10 to 40 μm. In comparing these results to the mercury intrusion results in Fig. 14, the IZ thickness most consistent with the experimental results would be 15–20 μm. While this value is somewhat smaller than the 40–50 μm typically measured using SEM techniques,[18,42,44] the larger pores would be expected to be present closest to the aggregate surface (since this is where the porosity is the largest

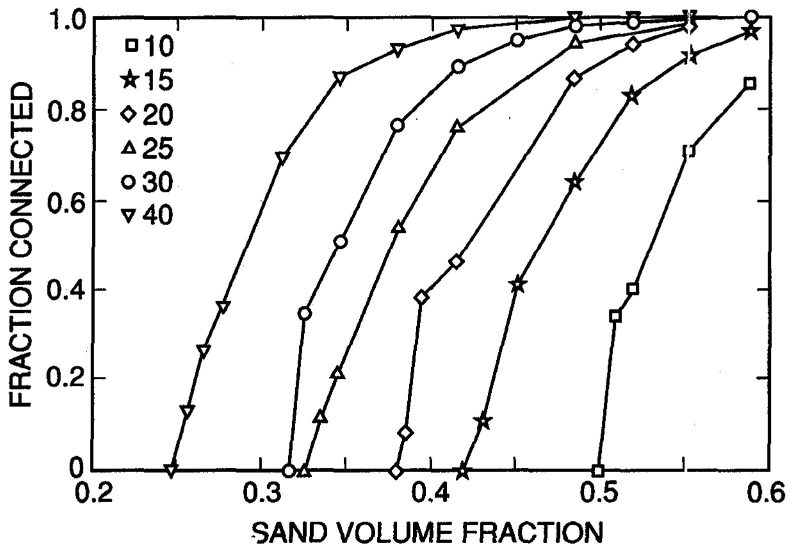

Fig. 15. Results of hard-core/soft-shell model used to determine interfacial zone percolation in mortars with varying sand contents and interfacial zone thicknesses. (Adapted from Ref. 20.)

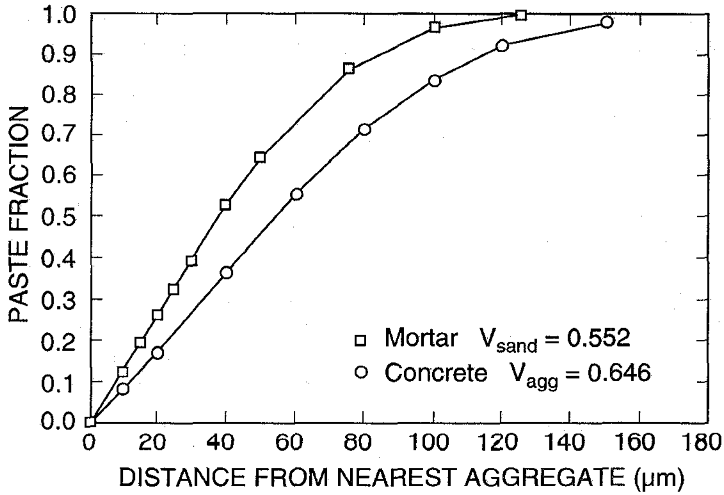

Fig. 16. Fraction of total cement paste within a given distance of aggregate. (Reprinted with permission from Ref. 20.)

both initially and after hydration) so that the IZ thickness detected by mercury intrusion should be less than that observed with the SEM. Uchikawa et al.[60] have applied a simpler analysis, based on the surface area of the aggregates, to mercury intrusion results for plain cement paste and concrete, and estimated an IZ thickness of 25–30 μm, in general agreement with the results presented here.

A version of the hard-core/soft-shell algorithm can also be used to determine the fraction of cement paste within a given distance of an aggregate surface in a typical mortar or concrete. Using aggregate size distributions given in Refs. 20 and 57, results shown in Fig. 16 indicate that nearly all of the cement paste is within 100 μm of an aggregate, consistent with the SEM-based observations of Diamond et al.[61] Additionally, 20–40% of the total cement paste is within the IZ regions or within 20–30 μm of an aggregate. This volume fraction of IZ paste is more than sufficient to create a percolated pathway through a typical mortar or concrete specimen,[20] suggesting that most field concrete will contain percolated IZ regions.

Effects of Interfacial Zones on Properties

Transport Properties

In a digital-image-based model as described above, the underlying digital image structure of the model microstructure is exploited to compute physical properties such as conductivity/diffusivity or fluid permeability. For instance, each pixel in the microstructure can be mapped into a finite element or a node in a finite difference scheme.[62] The appropriate equations can then be developed and boundary conditions applied to compute the physical quantity of interest for a specific microstructure. This requires, of course, that the relevant properties of the individual phases constituting the microstructure be known. These techniques have been applied in computing the diffusivity of cement paste as a function of water/cement ratio and degree of hydration by converting model microstructures into resistor networks and solving Laplace's equation.[63] The diffusivity is then obtained from the computed conductivity via the Nernst-Einstein equation.[63] This kind of simulation can be carried out on the digital-image models of the IZ, and effective properties can be computed for the IZ region. These effective properties can then be put into a higher-level model that treats cement paste as a continuum material. This two-step procedure has not yet been carried out, but we try to give some analysis below of experimental results that indicate the importance of the IZ for transport properties.

It is only recently that the issue of the effects of IZ microstructure and percolation on transport properties have been addressed experimentally in a systematic manner. Using simple geometries such as flat-plate aggregates or single or multiple circular aggregates, increases in conductivity,[64,65] chloride ion diffusivity,[66] and air permeability[67] due to the presence of IZ have been observed. Houst et al.[68] have studied the influence of aggregate content on the diffusion of gases in mortars and obtained evidence for IZ percolation between 49 and 55% volume fraction sand. Ping and Ming-shu have observed that the IZ in a quartz sand mortar allowed easier passage of aggressive ions than the bulk paste. However, in a cement clinker mortar, the IZ actually offered greater resistance to the passage of deleterious species than the bulk paste.[69] These transport results would be in agreement with the generally denser microstructure of the IZ in mortar with cement clinker aggregates.[52,54,55] Likewise, lightweight aggregate concretes have been shown to have very low permeabilities despite the possibly high permeabilities of the aggregates themselves.[70,71] In a lightweight concrete, the relatively dense IZ will separate the porous and permeable aggregates, producing a composite material with a low permeability. While by no means extensive, these results suggest both that IZ microstructure and percolation do significantly affect transport properties of concrete and that modification of IZ microstructure can improve the durability of concrete with respect to attack by transport-controlled processes (such as sulfate or chloride ion ingress).

Elastic Properties at the Cement Paste Level

Algorithms that perform finite-element simulations of cement paste elastic properties have only recently been developed. Some preliminary results will be discussed here, along with a brief discussion of how such simulations are carried out.

Starting with a model like the NIST cement paste microstructure model, each pixel is thought of as a cubic finite element. Simple trilinear finite elements[72] have proven to be adequate for simulating linear elastic properties. The corner of each pixel is then taken to be a node, at which elastic displacements are defined. A typical problem in three dimensions has 64^3–100^3 pixels (finite elements), which results in a memory requirement of 70–300 MB. The elastic equations are solved using an efficient conjugate gradient routine[73] to allow for reasonable run times for what would be considered a large finite element problem.[72] Each phase is assigned isotropic elastic moduli, which for crystals like CH can be determined from independent measurements.[74,75] Amorphous phases like C-S-H at present have to be calibrated by comparison with experiment.[76]

Some preliminary results for bulk cement paste are shown in Fig. 17 (p. 190), which shows a slice through the microstructure of a fully hydrated 0.245 water/cement-ratio C_3S paste, where white is C_3S, light gray is CH, dark gray is C-S-H, and black is water-filled capillary pore space. In the model, in order of decreasing stiffness, C_3S is most stiff, followed by CH, then C-S-H, then water. Figure 18(*a*) (p. 190) shows a color map of the trace of the stress matrix (essentially the total compressional stress), where red is high, green is medium, and gray through black is low stress. The image has been thresholded to show only the higher stresses. Figure 18(*b*) shows an image similar to Fig. 17, but with the C-S-H and pores eliminated by turning them black. It is clear by comparing Figs. 18(*a*) and (*b*) that the two stiffest phases, C_3S and CH, carry most of the stress. Figure 19(*a*) (p. 191) shows the dilational (trace of the strain tensor = volume change) strain for each pixel, with the same color scheme as in Fig. 18. The image has again been thresholded to eliminate the lower strains. Figure 19(*b*) shows the C-S-H and pore phases in white, with the C_3S and CH phases now blacked out. Comparison of Figs. 19(*a*) and (*b*) clearly shows that most of the dilatational strain is carried by the less stiff phases, as might be expected. Much more analysis of these results can be carried out, including studying the stress and strain distribution functions and individual phase contributions to the total elastic moduli. Figure 20(*a*) shows the stress distribution functions for each phase for the above microstructure, whereas Fig. 20(*b*) shows the equivalent strain distribution functions. The long tails in the stress distribution functions will be important in an analysis of fracture at the micrometer level, as the most highly stressed regions will be expected to crack first.

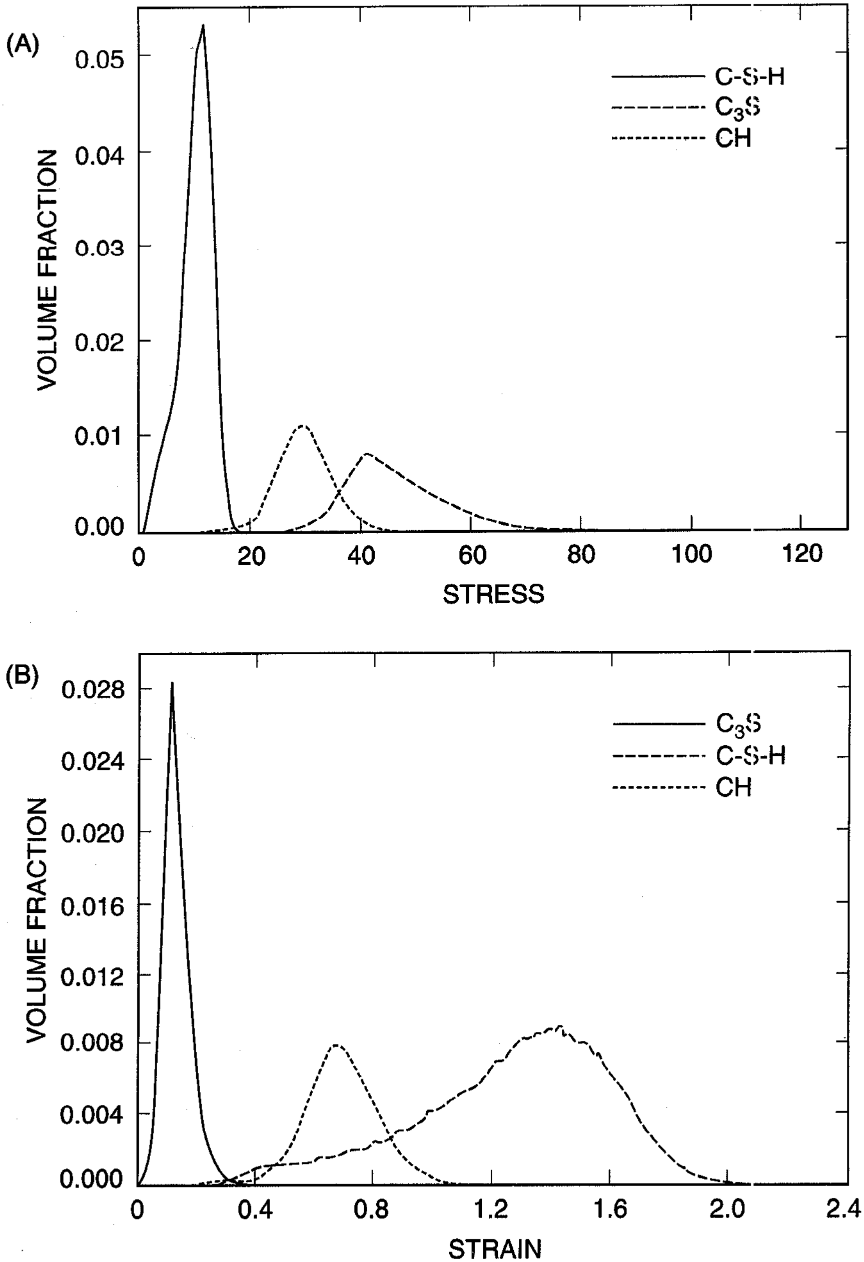

Fig. 20. Distribution functions computed from Fig. 17 microstructure for (*a*) compressional stress fields, and (*b*) dilatational strain fields.

By combining the above finite element analysis with the interfacial microstructure modeling work described earlier, it will be possible to study how the stress fields near an aggregate are affected by changes due to admixtures or aggregate properties. For example, it should be possible to make a determination of the effective elastic properties of the cement paste as a function of distance from the aggregate surface. Experimental measurements exist of the microhardness as a function of distance from the aggregate surface.[4,77–82] It is known that microhardness measurements can give some insight into elastic moduli.[83] Such continuum determinations, which effectively homogenize the cement paste, can then be incorporated into higher-level fracture models like the one that is described next.

Effects of Interfacial Zone Strength on Fracture in Concrete

Cracks in a heterogeneous material like concrete propagate in a direction perpendicular to the local maximum tensile stress, weighted by which direction has the easiest (lowest strength) route. In general then, the direction of crack propagation in concrete will be determined by the external (or internal) loading and the random distribution of elastic and fracture properties in the material. This distribution is a function of the arrangement of aggregate, paste, and IZ. In a normal-weight concrete, the IZ between the aggregates and the matrix is the weakest link.[84] In the Stevin Laboratory of Delft University a finite element lattice model, which operates directly on a digital image of microstructure, has been developed to simulate fracture in concrete.[85–89] The model treats cement paste as a uniform material, so it is a mesoscale model on the millimeter-length scale of aggregate particles. With the model, different fracture problems have been studied, including tensile[85,86] and shear[86,87] fracture, the pullout of anchor bolts,[88,90] and the effect of the IZ on the fracture mechanism of concrete.[86,91] This review concentrates on the last of these topics.

The model uses techniques that have recently received much attention in the statistical physics community.[92] The material is discretized as a two-dimensional lattice of linear elastic beam elements[86] and is used for plane stress simulations. A triangular shape for the lattice is chosen (Fig. 21), but other shapes are also possible (see Ref. 92). A regular triangular lattice is used in which all the beams have equal length and can transfer axial force, shear force, and bending moments, as shown schematically in Fig. 21. To solve the elastic equations, the finite element code DIANA[93] is used. Networks with truss elements, where free rotations are possible in the nodes, have also been used to investigate fracture in concrete.[94–96] Some three-dimensional simulations have been carried out recently.[97] To reduce computer time, only the parts of the specimen where cracks are expected to be present are modeled with the lattice. For the remainder of the specimen continuum, plane stress elements are used.

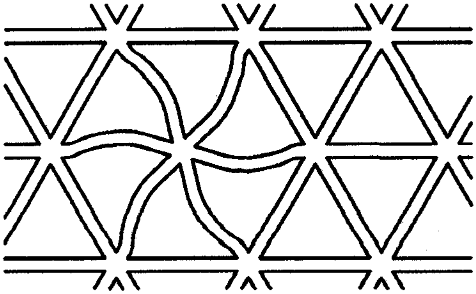

Fig. 21. Triangular lattice of beam elements. (Reprinted with permission from Ref. 85.)

In the linear elastic analysis, the specimen is loaded by giving nodal displacements or nodal loads. The outcomes of the linear elastic analysis are the normal forces, shear forces, and bending moments in the beams. In addition, the displacements of the nodes of the mesh and reaction forces in the supports can be retrieved from the analysis. In each step, the load is adjusted so that exactly one element has exceeded its prescribed tensile strength. Cracks are then propagated by removing this element.[86] After an element is removed, the next loading step is undertaken, followed by another element removal, until fracture is complete.

Different ways to implement heterogeneity are adopted as described in Ref. 86. One of them, which has some similarity to earlier work,[98] and which gives the best results when studying concrete fracture, will be discussed here. Concrete can be modeled as a three-phase material consisting of gravel aggregates embedded in a cement paste matrix joined by interfacial zones. Slices through spherical aggregates are generated randomly corresponding to known size distributions and using the correct three-dimensional-to-two-dimensional conversions.[86,99] An example is given in Fig. 22(*a*), with the maximum aggregate size (D_{max}) equal to 8 mm, and the aggregate volume fraction (P_k) equal to 0.75. Circles with small diameters (in this case smaller than 2 mm) are excluded from the generated grain structure because the length of the beam elements should be at least two or three times smaller than the smallest circle diameter to get accurate results.[86] Using smaller aggregate sizes increases the number of elements needed, making the simulation unacceptably slow for the computer that was used.[86] Faster computers and code modifications are available to overcome this limit. The triangular lattice is projected on top of the generated grain structure (Fig. 22(*a*)), and different strengths and stiffnesses are assigned to the respective beam elements (Fig. 22(*b*)) according to their locations in the microstructure. A beam element located on the boundary between aggregate and

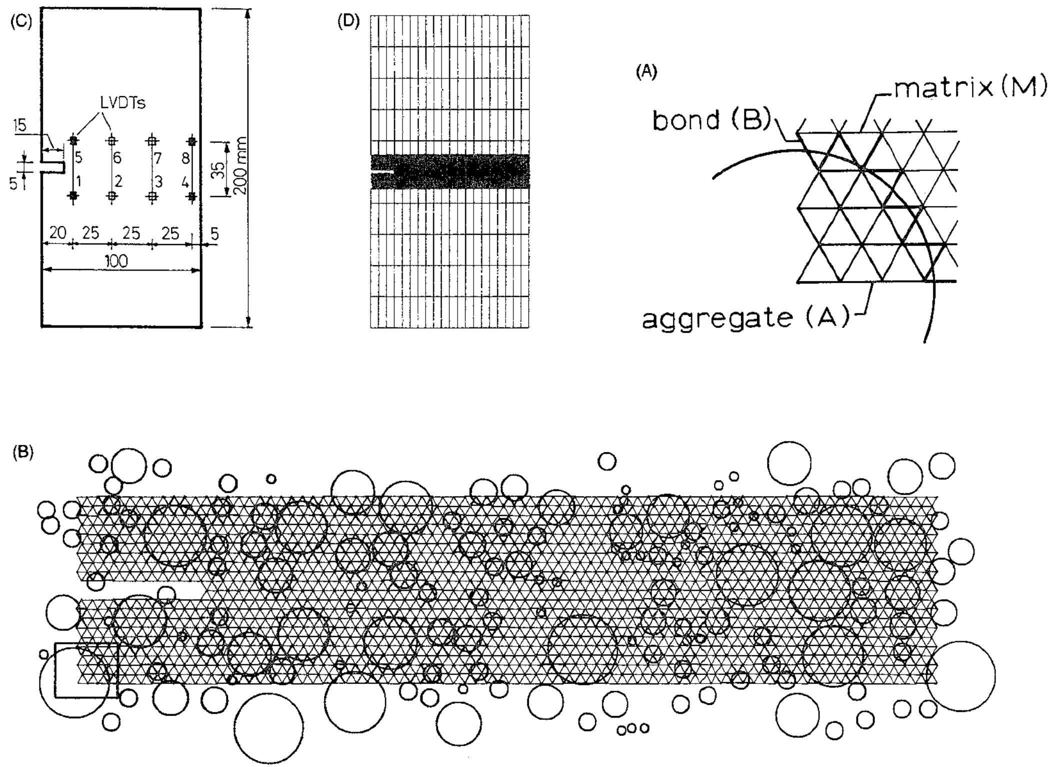

Fig. 22. (*a*) Triangular lattice projected on the generated concrete microstructure. (*b*) Definition of aggregate, bond, and matrix beams. (*c*) Single-edge-notched specimen used for impregnation experiments. (*d*) Mesh used in simulations. (Reprinted with permission from Ref. 85.)

matrix is classified as an IZ element, and so will get a low bond strength when normal-weight concrete is simulated. In all of these simulations, Poisson's ratio was set at 0.16 for all three phases.

Tensile Loading Simulations

Experiments on single-edge-notched plates loaded in uniaxial tension between nonrotating end platens have been carried out.[100,101] The specimen dimensions are shown in Fig. 22(*c*). In Fig. 23(*a*), the load-displacement diagrams for normal-weight concrete and mortar loaded up to maximum displacements of w equal to 25 and 100 μm are shown. It was concluded[100,101] that up to a displacement of about 50 μm, the crack is still propagating through the specimen's cross section. At larger displacements, the crack traverses the specimen completely but is not continuous—overlaps with intact ligaments in between, called crack face bridges, can be observed in Fig. 23(*b*). This implies that loads can still be transferred between the crack faces. For larger aggregate particles in the concrete, the overlaps are larger, which results in larger bridging stresses and thus a higher tail in the load-displacement response. The long tail in the softening diagram can probably be explained by a large deformation between the crack faces through bending of the bridges.

The above experiments have been simulated with the fracture model, with the mesh used given in Fig. 22(*d*). The specimen is loaded vertically by prescribing the boundary displacements. Four simulations were performed with different input parameters for the beam elements. Table I gives the input parameters for these simulations. The crack history for simulation I is given in

Table I. Input Parameters for Simulations of Uniaxial Tensile Tests

	Analysis Number			
	I	II	III	IV
E_A (GPa)	70	70	70	25
E_M (GPa)	25	25	25	25
E_B (GPa)	25	25	25	25
σ_A (MPa)	10	10	10	1
σ_M (MPa)	5	5	5	5
σ_B (MPa)	0.5	1	2.5	2

Note: A = aggregate
B = interfacial zone
M = matrix
E = Young's modulus
σ = tensile strength
Aggregate size is between 2 and 8 mm.

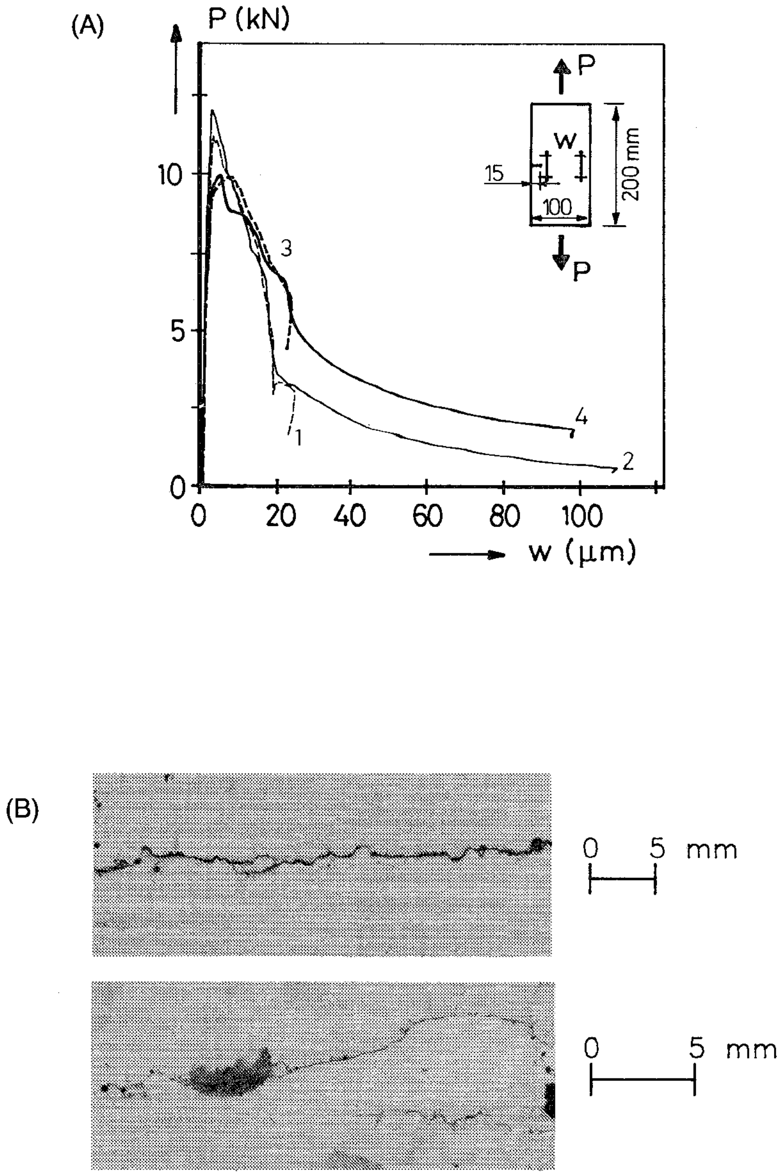

Fig. 23. (*a*) Load-displacement curves for normal-weight concrete (curves 3 and 4) and mortar (curves 1 and 2) specimens loaded to maximum displacements of w = 25 and 100 μm; (*b*) crack face bridges in concrete and mortar (according to Van Mier[100,101]). (Reprinted with permission from Ref. 101.)

Fig. 24. The load-displacement curve is plotted in Fig. 25. In this curve, the places are marked where the pictures of the crack history are made. It can be concluded that microcracking over the entire cross section starts before the maximum load is reached (Fig. 24(*a*)). After peak load the crack starts to localize in one main crack (Fig. 24(*b*)). Notice that the main crack starts at the unnotched side of the specimen. This phenomenon has also been observed in some of the experiments.[100,101] A combination of bending moments, which occur due to the fixed end platen, and microstructural randomness (in the simulated mesh there are more large aggregate particles located at the unnotched side) probably causes this effect. At the beginning of the long tail in the descending branch, the cross section is almost completely cracked (Fig. 24(*c*)). Small intact material pieces bridging the crack faces are the reason for the long tail in the load-displacement curve (Fig. 24(*d*)). In simulations II and III, higher strengths are given to the elements in the interfacial zone. From Fig. 26, where the final crack patterns for the four simulations are plotted, it is clearly visible that, with increasing bond strength, less microcracking occurs outside the main crack path, and the number of bridges decreases. In simulation IV, the strength of the beams inside the aggregates is taken smaller than the bond and matrix beams in order to simulate fracture in lightweight concrete. In this case, the aggregates crack first, as seen in Fig. 26. In addition, crack face bridges are observed *inside* the aggregates, which is in agreement with experimental observations.[100,101]

Shear Loading Simulations

The fracture model has also been used to investigate the influence of the IZ strength on the overall specimen strength in four-point shear experiments on double-edge-notched beams.[86,91] The specimen geometry matches that of Bazant and Pfeiffer,[102] who claimed that a "true shear crack" (defined as a regular array of inclined microcracks) had developed in these beams. However the tests have recently been duplicated, using the same geometry, but with a different loading device with well-known boundary conditions.[86] These later experiments have shown that rather than a shear crack, a curved mode I crack is developed in the four-point shear specimen, as seen in Fig. 27(*a*). For the simulations, a specimen of 75-mm width and 37.5-mm thickness was used, with the input parameters as given in Table II. Nine different values for the strength of the beam elements in the IZ were used, ranging from 0.1 to 1 times the cement paste matrix strength. In Figs. 27 (*b–d*), the crack patterns of three beams with different bond strengths are shown. Table II gives the maximum load values for the nine simulations. It can be concluded that if the IZ strength is increased, the number of microcracks outside the main crack is reduced. The result agrees with the simulations of the uniaxial tensile tests presented above.

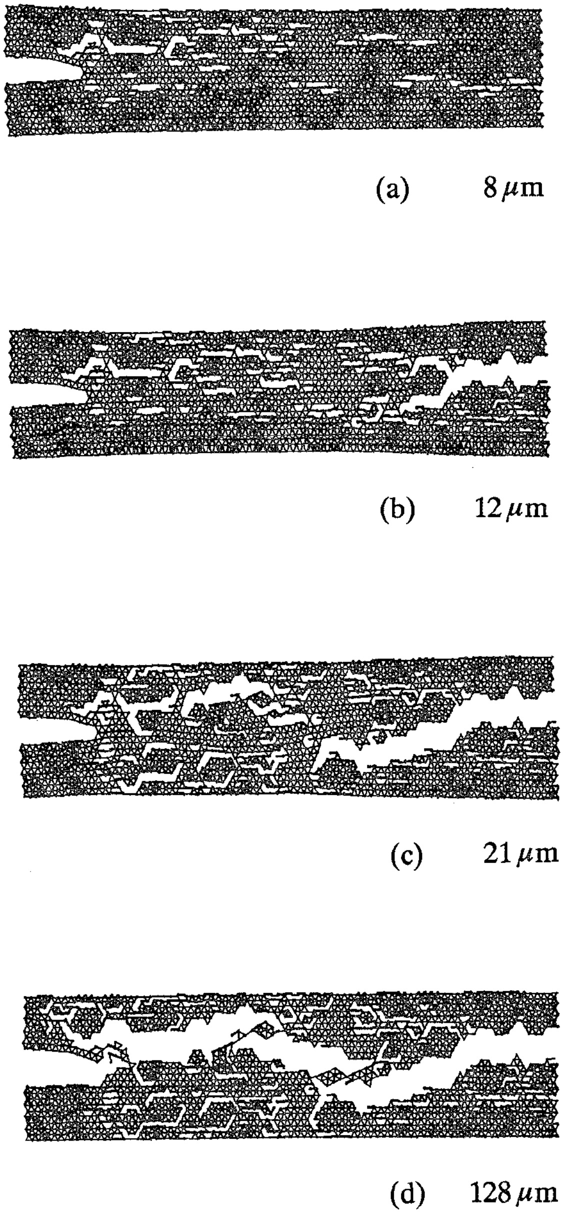

Fig. 24. Crack history for simulation I shown at four different displacements *w*: (*a*) 8 μm, (*b*) 12 μm, (*c*) 21 μm, and (*d*) 128 μm. (Reprinted with permission from Ref. 85.)

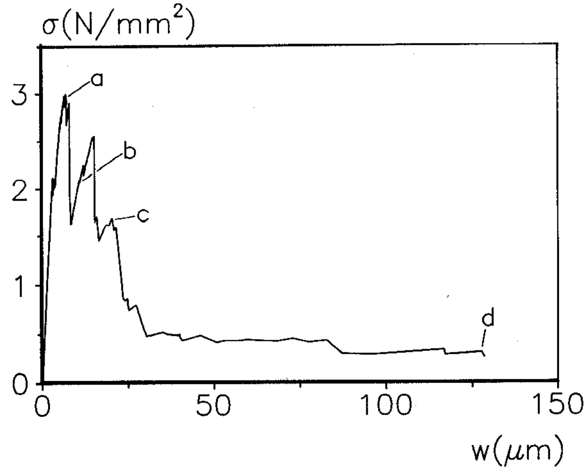

Fig. 25. Stress (σ) vs displacement (w) response for simulation I. The crack patterns in Fig. 24 were plotted at the four marked stages, (a), (b), (c), and (d). (Reprinted with permission from Ref. 85).

Table II. Input Parameters and Peak Loads for the Nine Simulations of Four-Point Shear Test

	Analysis Number								
	1	2	3	4	5	6	7	8	9
σ_B (MPa)	1.25	0.5	0.75	1.0	1.5	1.75	2.0	3.0	5.0
P_{max} (kN)	14.3	14.6	14.7	12.6	14.3	15.6	16.4	17.8	19.4

Note: A = aggregate
B = interfacial zone
M = matrix
E = Young's modulus
σ = tensile strength
P_{max} = maximum load applied
Aggregate size is between 3 and 8 mm.
Tensile strength: σ_A = 10 MPa, σ_M = 5 MPa
Young's modulus: E_A = 70 GPa, E_M = 25 GPa, E_B = 25 GPa

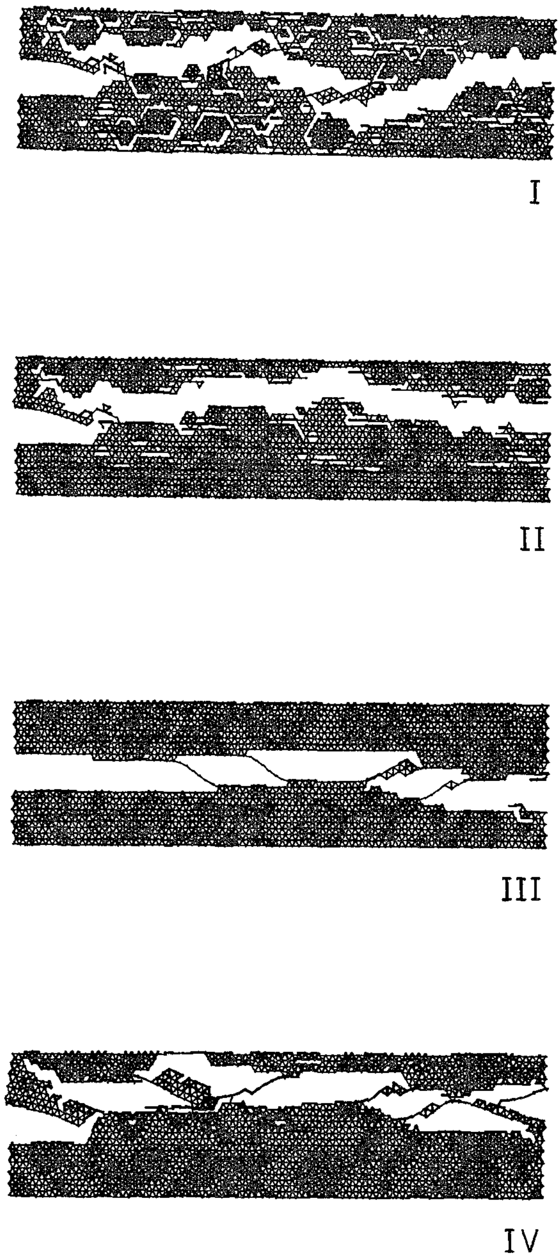

Fig. 26. Final (maximum displacement) crack patterns for four different tensile test simulations. The parameters for each *simulation* are given in Table I. (Reprinted with permission from Ref. 85.)

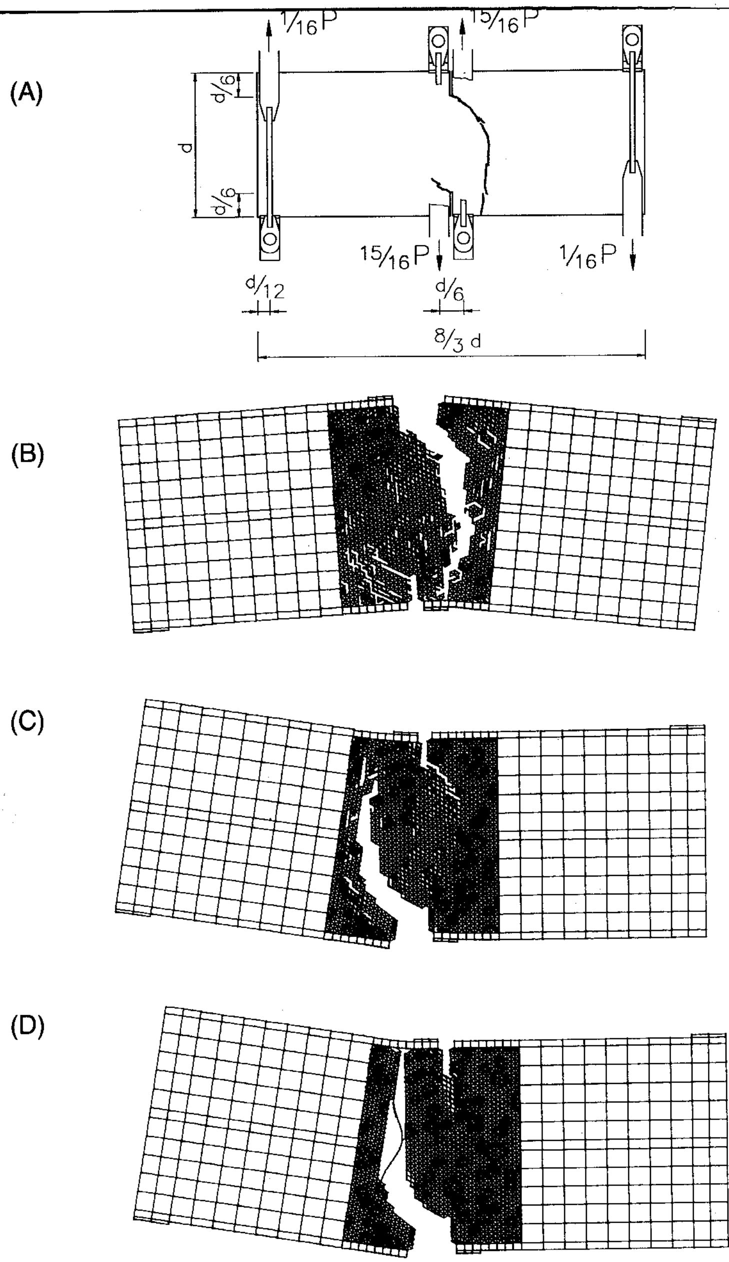

Fig. 27. Experimental crack pattern (*a*) for four-point shear beam (reprinted with permisssion from Ref. 87), and three simulated crack patterns for bond strengths of (*b*) 0.5 MPa, (*c*) 1.5 MPa, and (*d*) 5.0 MPa.

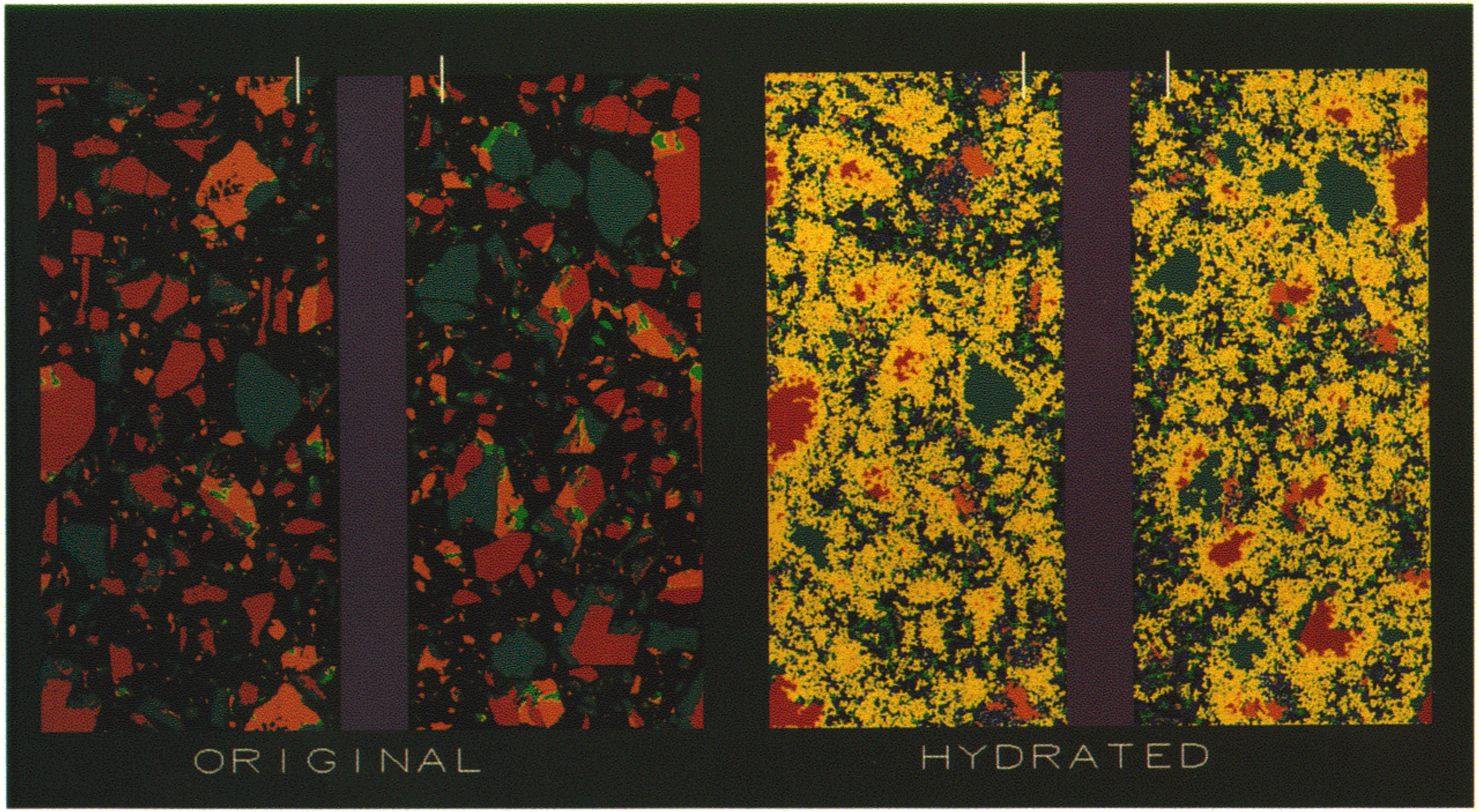

Fig. 1. Computer-generated images of actual cement particles placed around a flat plate aggregate before and after hydration. In the image before hydration, the aggregate is magenta, C_3S is red, C_2S is blue, C_4AF is orange, C_3A is bright green, gypsum is dull green, and water-filled porosity is black. In the image after hydration, C-S-H gel is yellow, CH is dark blue, and aluminate hydration products (Aft, Afm, C_3AH_6) are green. (Reprinted from Ref. 9.)

Fig. 3. Illustration of NIST cement microstructure development model showing from left to right initial particles, dissolution phase of hydration cycle, diffusion phase of hydration cycle, microstructure at 32% hydration, and microstructure at 76% hydration. Colors are the same as in Fig. 1. (Adapted from Ref. 62.)

There is less crack branching for increasing strength of the IZ elements. For this loading, the total load that can be carried by the specimen was dependent on the IZ strength. An increase of a factor of ten in the IZ strength gave an increase of specimen strength of 30–35%. The densification of the interfacial zone seen in experiment and simulation could certainly increase the strength of the IZ by this kind of factor. This is an area in which more research is needed. It may then be concluded that the specimen strength is governed mainly by the matrix strength, in agreement with experimental data.[103] In Fig. 27 it can be seen that the crack starts at either the top or the bottom notch, depending on the IZ strength and the position of the aggregate particles.

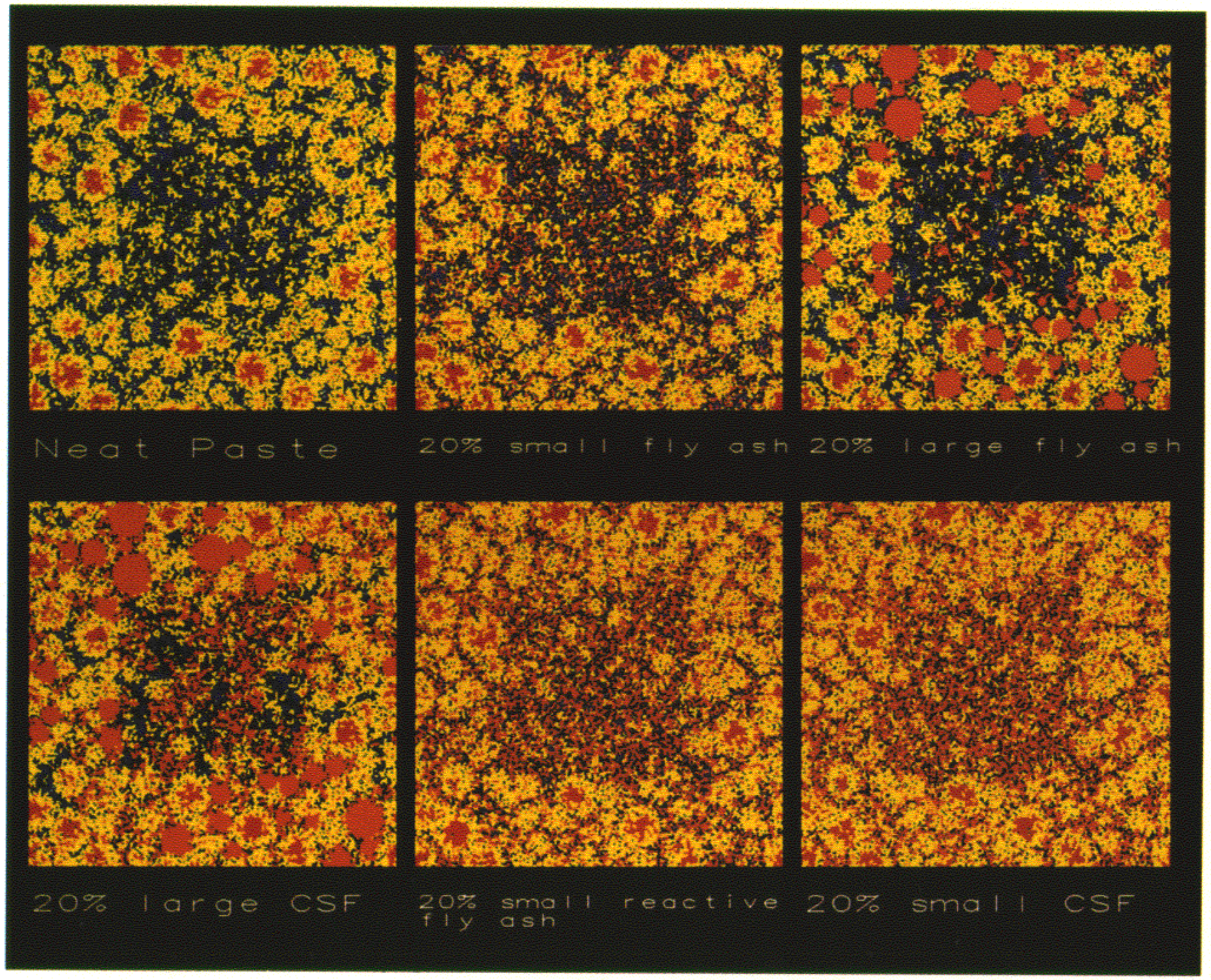

Fig. 7. Interfacial zone microstructures for C_3S cement pastes containing various mineral admixtures (water/solid ratio = 0.45, 77% hydration). C_3S is red, C-S-H gel is yellow, CH is blue, pozzolanic material (mineral admixture and C-S-H) is tan, and porosity is black.

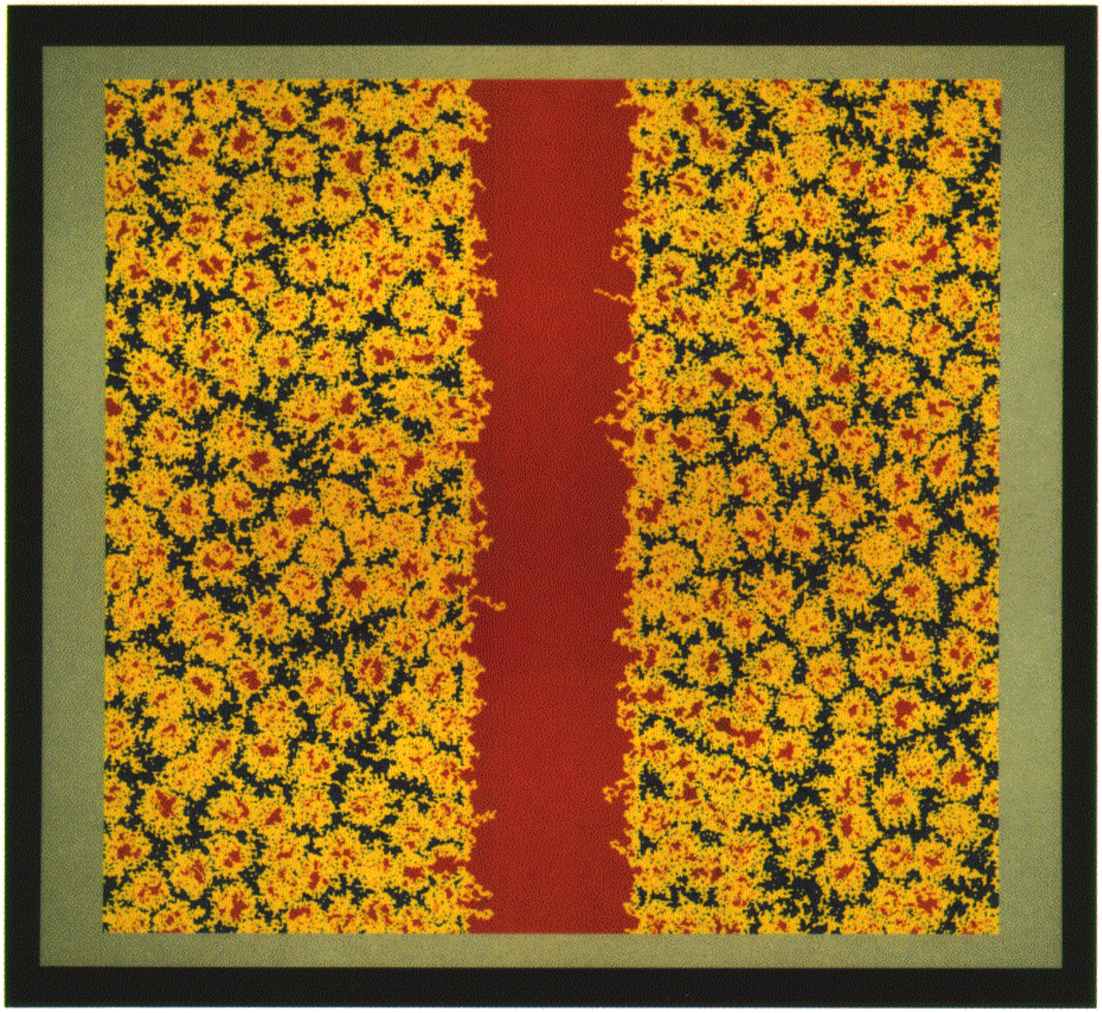

Fig. 12. Hydrated microstructure for an absorptive clinker aggregate at 75% hydration. (Adapted from Ref. 36.)

Summary and Needed Research

This chapter has reviewed recent fundamental computer modeling work[6] on both the microstructure of the IZ and its effect on properties. The modeling approach followed was to, at each length scale of interest, directly represent the microstructural features that determine properties. Once microstructure was numerically represented, properties could then be computed. In this approach, because of computational limitations and the seven orders of magnitude of feature size in concrete, each length scale was studied by a different model, with results from models at smaller length scales being used in higher-length-scale models. This approach to concrete, in its ideal realization, is now summarized.

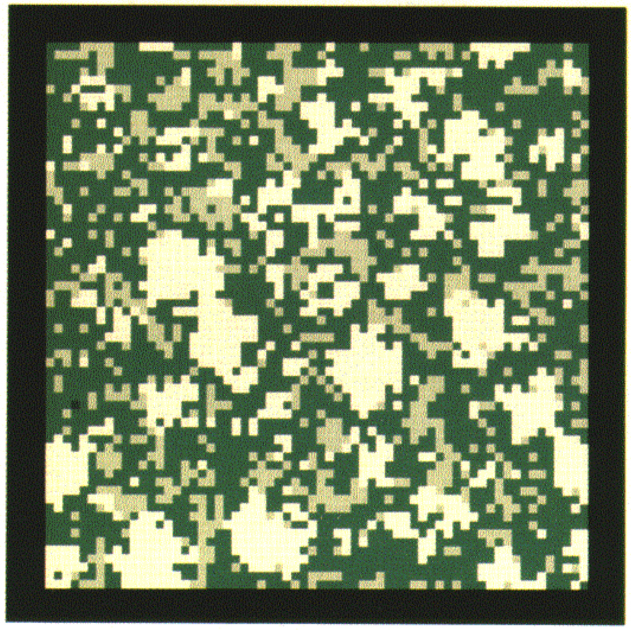

Fig. 17. Slice through microstructure of simulated 0.25 water/cement paste. White is C_3S, light gray is CH, dark gray is C-S-H, and black is capillary pores.

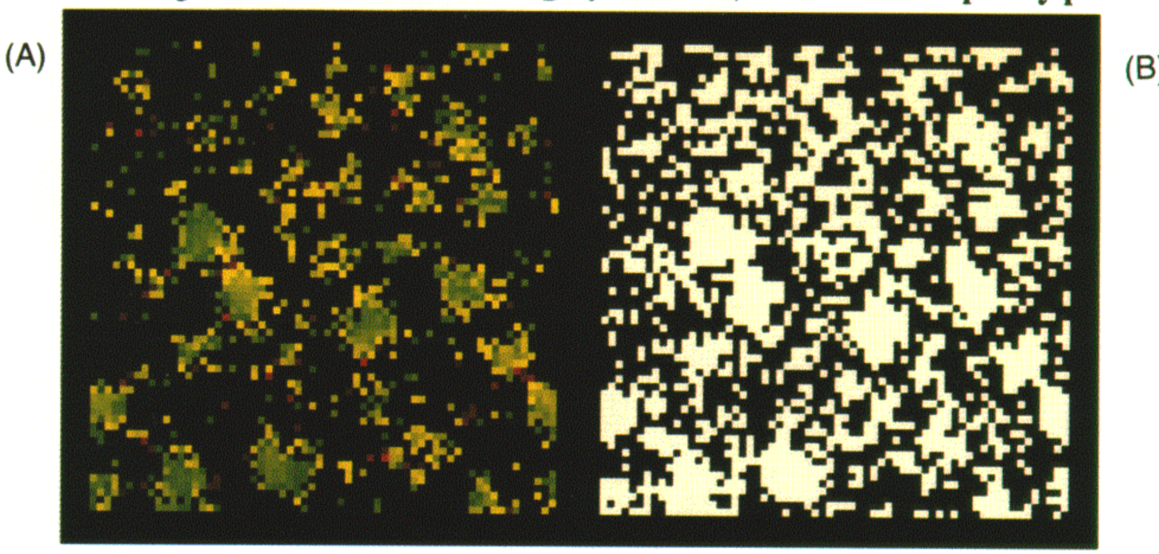

Fig. 18. (*a*) Compressional stress fields for microstructure shown in Fig. 17 (red is high, yellow is medium, gray through black is low); (*b*) microstructure shown in Fig. 17, but with C_3S and CH white, other phases are black.

(A) 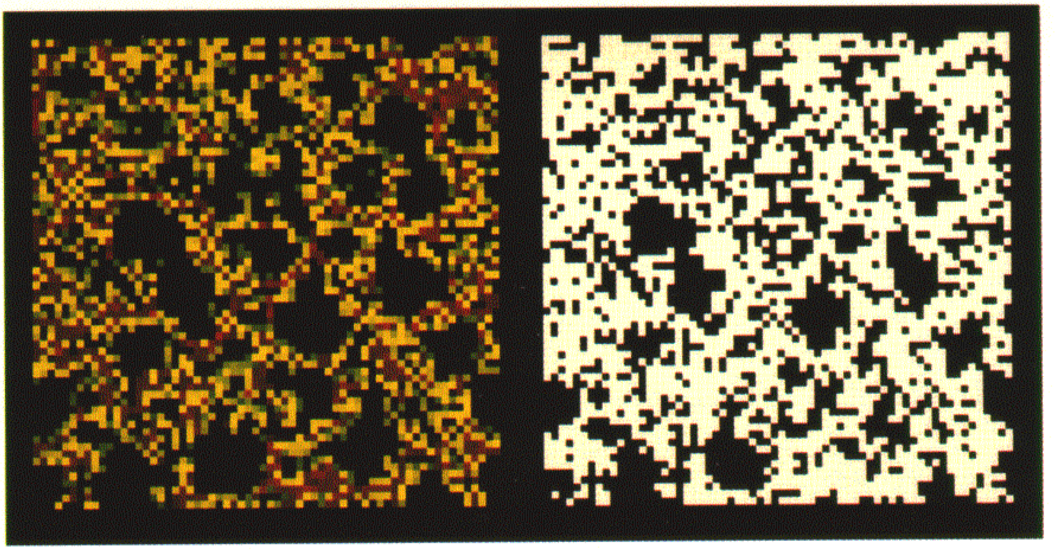 (B)

Fig. 19 (*a*) Dilatational strain fields for microstructure shown in Fig. 17 (red is high, yellow is medium, gray through black is low); (*b*) microstructure shown in Fig. 17, but with C-S-H and pores white, other phases are black.

First, random atomic, molecular, and molecular cluster-scale models are used to rigorously compute the structure and properties of C-S-H and other nanometer-scale gel materials in portland cement paste. Lattice calculations are also carried out for the crystalline phases, such as CH. Theoretical results are validated against experimental results. These phases are then treated as continuum materials with known properties in a micrometer-scale cement paste model, such as the NIST cement paste model. Using this kind of model, properties are again computed exactly, within numerical error. IZ properties are also computed for a single aggregate-cement paste interface. Cement paste is then treated as a continuum with known properties in a millimeter-scale model for mortar or concrete, as in the fracture model described earlier, for both bulk cement paste and IZ cement paste. If necessary, fine aggregate can be handled in a millimeter-scale model for mortar. Mortar can then be treated as a continuum material with known properties in a centimeter-scale concrete model. This last step would be only out of computational necessity, since it would be unsatisfactory to treat fine aggregate and coarse aggregate separately simply because of a size difference between them.

The research presented in this chapter clearly shows that there are holes in the above systematic approach that need to be filled in. For example, there is no published work to date on molecular-dynamic-type models for the nanometer-scale structure of C-S-H. That means that values of property coefficients (e.g., transport coefficients) have to be inferred by comparison to experimental results.[63] Micrometer-scale models of linear elastic properties are being actively worked on,[76] but fracture behavior at this level has not been modeled. Transport at the millimeter scale has not been modeled, although the micrometer-scale information (with nanometer-scale information fitted from experimental results) is available for some transport processes. The next five years should see these areas being filled in, with possibly great increases in understanding attainable as the different length scales in concrete are linked together in a scientifically rigorous way.[104] This chapter has demonstrated the potential of this approach for understanding the role of interfacial zones in determining the properties of concrete.

Acknowledgments

The above comprehensive, systematic approach to modeling the microstructure and properties of concrete is being supported at NIST via the NIST/ACBM Cementitious Materials Modelling Laboratory (CMML). The CMML provides for archiving of models, and publishes a newsletter on modeling developments. D.P.B. and E.J.G. would like to thank the National Science Foundation and Technology Center for Advanced Cement-Based Materials and R.J. Lee Group, Inc., for partial financial support of this work. The work of E.S. has been made possible through a grant of the Dutch Technology Foundation and by a fellowship of the Royal Netherlands Academy of Arts and Sciences. We would also like to thank our collaborators in research on interfacial zones: D.N. Winslow and M.D. Cohen at Purdue University, P.V. Coveney and M.F. Kleyn at Schlumberger Cambridge Research, A.R. Day at Marquette University, K.A. Snyder and P.E. Stutzman at NIST, and J.G.M. Van Mier at Delft University, who guided the Ph.D. research of E.S. on the lattice fracture model. We would also like to thank H.M. Jennings of Northwestern University for useful discussions concerning the interactions between models at different length scales.

References

[1]*Interfaces in Cementitious Composites*. Edited by J.C. Maso. E & FN Spon, London, 1992.

[2]L. Struble, J.P. Skalny, and S. Mindess, "A Review of the Cement-Aggregate Bond," *Cem. Concr. Res.*, **10**, 277–86 (1980).

[3]D. Breton, A. Carles-Gibergues, G. Ballivy, and J. Grandet, "Contribution to the Formation Mechanism of the Transition Zone Between Rock-Cement Paste," *Cem. Concr. Res.*, **23**, 335–46 (1993).

[4]J.A. Larbi, "Microstructure of the Interfacial Zone Around Aggregate Particles in Concrete," *HERON*, **38** [1] 1–69 (1993).

[5]A. Bentur, "The Role of the Interface in Controlling the Performance of High-Quality Cement Composites"; pp. 227–37 in *Advances in Cement Manufacture and Use*. Edited by E.M. Gartner. Engineering Foundation, New York, 1989.

[6]E.J. Garboczi and D.P. Bentz, "Fundamental Computer Simulation Models for Cement-Based Materials"; pp. 249–77 in *Materials Science of Concrete II*. Edited by J. P. Skalny and S. Mindess. The American Ceramic Society, Westerville, OH, 1991.

[7]E.J. Garboczi, "Computational Materials Science of Cement-Based Materials," *Mater. Struct.*, **26**, 191–5 (1993).

[8]D.P. Bentz and E.J. Garboczi, "Digital-Image-Based Computer Modelling of Cement-Based Materials"; pp. 44–51 in *Digital Image Processing: Techniques and Applications in Civil Engineering*. Edited by J.D. Frost and J.R. Wright. American Society of Civil Engineers, New York, 1993.

[9]D.P. Bentz and P.E. Stutzman, "SEM Analysis and Computer Modelling of Hydration of Portland Cement Particles"; pp. 60–73 in *Petrography of Cementitious Materials*, ASTM STP 1215. Edited by Sharon M. Dehayes and David Stark. ASTM, Philadelphia, 1994.

[10]P.E. Stutzman, "Serial Sectioning of Hardened Cement Paste for Scanning Electron Microscopy"; pp. 237–49 in *Ceramic Transactions, Volume 16: Advances in Cementitious Materials*. Edited by Sidney Mindess. The American Ceramic Society, Westerville, OH, 1991.

[11]B.P. Flannery, H.W. Deckman, W.G. Roberge, and K.L. D'Amico, "Three-Dimensional X-ray Microtomography," *Science*, **237**, 1439–44, 1987.

[12]L.W. Schwartz, F. Auzerais, J. Dunsmuir, N. Martys, D.P. Bentz, and S. Torquato, "Transport and Diffusion in Three-Dimensional Composite Media," *Physica A*, **207**, 28–36 (1994).

[13]D.P. Bentz, P. Coveney, E.J. Garboczi, M. Kleyn, and P.E. Stutzman, "Cellular Automaton Simulations of Cement Hydration and Microstructure Development," *Modelling and Simulation in Materials Science and Engineering*, (July 1994).

[14]S. Mindess and J.F. Young, *Concrete*, Prentice-Hall, Englewood Cliffs, NJ, 1981.

[15]J.F. Young and W. Hansen, "Volume Relationships for C-S-H Formation Based on Hydration Stoichiometry"; pp. 313–22 in *Microstructural Development During Cement Hydration*. Edited by L.J. Struble and P.W. Brown. Materials Research Society, Pittsburgh, 1987.

[16]P. Lu, G.K. Sun, and J.F. Young, "Phase Composition of Hydrated DSP Cement Pastes," *J. Am. Ceram. Soc.*, **76** [4] 1003–7 (1993).

[17]K.L. Scrivener, "The Microstructure of Concrete," pp. 127–61 in *Materials Science of Concrete I*. Edited by J. P. Skalny. The American Ceramic Society, Westerville, OH, 1989.

[18]K.L. Scrivener and E.M. Gartner, "Microstructural Gradients in Cement Paste Around Aggregate Particles"; pp. 77–85 in *Bonding in Cementitious Materials*. Edited by S. Mindess and S. Shah. Materials Research Society, Pittsburgh, 1988.

[19]S. Torquato, "Bulk Properties of Two-Phase Disordered Media, 1. Cluster Expansion for the Dielectric Constant of Dispersions of Penetrable Spheres," *J. Chem. Phys.*, **81**, 5079–88 (1984).

[20]D.N. Winslow, M.D. Cohen, D.P. Bentz, K.A. Snyder, and E.J. Garboczi, "Percolation and Pore Structure in Mortars and Concrete," *Cem. Concr. Res.*, **24**, 25–37 (1994).

[21]J. Farran, "Contribution Mineralogique a L'etude de L'adherence Entre les Constituants Hydrates des Ciments et les Materiaux Enrobes," *Rev. Mater. Constr.*, **490-491**, 155–72 (1956).

[22]B.D. Barnes, S. Diamond, and W.L. Dolch, "The Contact Zone Between Portland Cement Paste and Glass Aggregate Surfaces," *Cem. Concr. Res.*, **8**, 233–44 (1978).

[23]R. Zimbelmann, "A Contribution to the Problem of Cement-Aggregate Bond," *Cem. Concr. Res.*, **15**, 801–8 (1985).

[24]C.Z. Yuan and I. Odler, "The Interfacial Zone Between Marble and Tricalcium Silicate Paste," *Cem. Concr. Res.*, **17**, 784–92 (1987).

[25]B.D. Barnes, S. Diamond, and W.L. Dolch, "Micromorphology of the Interfacial Zone Around Aggregates in Portland Cement Mortar," *J. Am. Ceram. Soc.*, **62**, 21–4 (1979).

[26]M. Hoshino, "Difference of the W/C Ratio, Porosity, and Microscopical Aspect Between the Upper Boundary Paste and the Lower Boundary Paste of the Aggregate in Concrete," *Mater. Struct.*, **21**, 336–40 (1988).

[27]P.J.M. Monteiro, O.E. Gjorv, and P.K. Mehta, "Microstructure of the Steel-Cement Paste Interface in the Presence of Chloride," *Cem. Concr. Res.*, **15**, 781–4 (1985).

[28]A.M. Zayed, "The Nature of the Concrete-Steel Rebar Interface in Plain and Silica Fume Concrete"; pp. 341–7 in *Advanced Cementitious Systems: Mechanisms and Properties*. Materials Research Society, Pittsburgh, 1992.

[29]R.J. Detwiler, P.J.M. Monteiro, H.R. Wenk, and Z. Zhong, "Texture of Calcium Hydroxide Near the Cement Paste-Aggregate Interface," *Cem. Concr. Res.*, **18**, 823–9 (1988).

[30]P.J.M. Monteiro and P.K. Mehta, "Ettringite Formation on the Aggregate-Cement Paste Interface," *Cem. Concr. Res.*, **15**, 378–80 (1985).

[31]E.J. Garboczi and D.P. Bentz, "Digital Simulation of the Aggregate-Cement Paste Interfacial Zone in Concrete," *J. Mater. Res.*, **6** [1] 196–201 (1991).

[32]M.W. Grutzek, D. Shi, G. Liu, and S. Kwan, "Computer Simulation of Interfacial Packing in Concrete," *J. Mater. Sci.*, **28**, 3444–50 (1993).

[33]J.A. Larbi and J.M.J.M. Bijen, "Effects of Water-Cement Ratio, Quantity and Fineness of Sand on the Evolution of Lime in Set Portland Cement Systems," *Cem. Concr. Res.*, **20**, 783–94 (1990).

[34]M. Saito and M. Kawamura, "Effect of Fly Ash and Slag on the Interfacial Zone Between Cement and Aggregate"; pp. 669–88 in *Fly Ash, Silica Fume, and Natural Pozzolans in Concrete*, ACI SP 114. Edited by V.M. Malhotra. ACI, Detroit, 1989.

[35]J.C. Maso, "The Bond Between Aggregates and Hydrated Cement Pastes"; pp. 3–15 in *Proceedings of the Seventh International Congress on the Chemistry of Cement*, 1980.

[36]D.P. Bentz, E.J. Garboczi, and P.E. Stutzman, "Computer Modelling of the Interfacial Zone in Concrete"; pp. 107–16 in *Interfaces in Cementitious Composites*. Edited by J.C. Maso. E & FN Spon, London, 1992.

[37]W.G. Cochran, *Sampling Techniques*. J. Wiley & Sons, New York, 1963.

[38]K. van Breugel, "Simulation of Hydration and Formation of Structure in Hardening Cement-Based Materials"; Ph. D. Thesis, Delft Univesity of Technology, The Netherlands, 1991.

[39]D.P. Bentz and E.J. Garboczi, "Simulation Studies of the Effects of Mineral Admixtures on the Cement Paste-Aggregate Interfacial Zone," *ACI Mater. J.*, **88**, 518–29 (1991).

[40]R.D. Hooton, "Permeability and Pore Structure of Cement Paste Containing Fly Ash, Slag, and Silica Fume"; pp. 128–43 in *Blended Cements*. Edited by G. Frohnsdorff. ASTM, Philadelphia, 1986.

[41]K.L. Scrivener, A. Bentur, and P.L. Pratt, "Quantitative Characterization of the Transition Zone in High Strength Concretes," *Adv. Cem. Res.*, **1** [4] 230–7 (1988).

[42]A. Bentur and M.D. Cohen, "Effect of Condensed Silica Fume on the Microstructure of the Interfacial Zone in Portland Cement Mortars," *J. Am. Ceram. Soc.*, **70** [10] 738–43 (1987).

[43]P.J.M. Monteiro, O.E. Gjorv, and P.K. Mehta, "Effect of Condensed Silica Fume on the Steel-Cement Paste Transition Zone," *Cem. Concr. Res.*, **19**, 114–23 (1989).

[44]D.P. Bentz, P.E. Stutzman, and E.J. Garboczi, "Experimental and Simulation Studies of the Interfacial Zone in Concrete," *Cem. Concr. Res.*, **22**, 891–902 (1992).

[45]E.E. Berry, R.T. Hemmings, W.S. Langley, and G.G. Carrette, "Beneficiated Fly Ash: Hydration, Microstructure, and Strength Development in Portland Cement Systems"; pp. 241–73 in *Fly Ash, Silica Fume, and Natural Pozzolans in Concrete*, ACI SP 114. Edited by V.M. Malhotra. ACI, Detroit, 1989.

[46]F. Sybertz, "Comparison of Different Methods for Testing the Pozzolanic Activity of Fly Ashes"; pp. 477–97 in *Fly Ash, Silica Fume, and Natural Pozzolans in Concrete*, ACI SP 114. Edited by V.M. Malhotra. ACI, Detroit, 1989.

[47]S. Slanicka, and S. Lamacska, "The Influence of Fly Ash Fineness on the Strength of Concrete," *Cem. Concr. Res.*, **21**, 285–96 (1991).

[48]H.A.W. Cornelissen and C.H. Gast, "Upgrading of PFA for Utilization in Concrete"; pp. 457–70 in *Fly Ash, Silica Fume, and Natural Pozzolans in Concrete*, ACI SP 114. Edited by V.M. Malhotra. ACI, Detroit, 1992.

[49]M.H. Zhang, and O.E. Gjorv, "Microstructure of the Interfacial Zone Between Lightweight Aggregate and Cement Paste," *Cem. Concr. Res.*, **20**, 610–18 (1990).

[50]T.A. Holm, T.W. Bremner, and J.B. Newman, "Lightweight Aggregate Concrete Subject to Severe Weathering," *Concr. Int.*, **6**, 49–54, June 1984.

[51]G. Fagerlund, "Frost Resistance of Concrete with Porous Aggregate," Report of the Cement and Concrete Institute in Sweden, 1978.

[52]R.L. Berger, "Properties of Concrete with Cement Clinker Aggregate," *Cem. Concr. Res.*, **4**, 99–112 (1974).

[53]R. Zimbelmann, "A Method for Strengthening the Bond Between Cement Stone and Aggregates," *Cem. Concr. Res.*, **17**, 651–60 (1987).

[54]S. Yang, X. Zhongzi, X. Ping, and T. Mingshu, "A New Method of Enhancing Cement-Aggregate Interfaces. I. Ideal Aggregate and Its Effects on Interfacial Microstructures," *Cem. Concr. Res.*, **22**, 612–8 (1992).

[55]S. Yang, X. Zhongzi, X. Ping, and T. Mingshu, "A New Method of Enhancing Cement-Aggregate Interfaces. II. Mechanical Properties and Sulphate Attack Resistances of Mortars," *Cem. Concr. Res.*, **22**, 769–73 (1992).

[56]K. Mitsui, Z. Li, D.A. Lange, and S.P. Shah, "A Study of Properties of the Paste-Aggregate Interface"; pp. 119-128 in *Interfaces in Cementitious Composites*. Edited by J.C. Maso. E & FN Spon, London, 1992.

[57]D. Winslow and D. Lui, "The Pore Structure of Paste in Concrete," *Cem. Concr. Res.*, **20**, 227 (1990).

[58]A.J. Katz and A.H. Thompson, "Quantitative Prediction of Permeability in Porous Rock," *Phys. Rev. B*, **34**, 8179–81 (1986).

[59]R.F. Feldman, "The Effect of Sand/Cement Ratio and Silica Fume on the Microstructure of Mortars," *Cem. Concr. Res.*, **16**, 31–9 (1986).

[60]H. Uchikawa, S. Hanehara, and D. Sawaki, "Relationship Between Thickness of Transition Zone and Strength of Hardened Mortar and Concrete"; presented at the 94th Annual Meeting of the American Ceramic Society, Minneapolis, 1992.

[61]S. Diamond, S. Mindess, and J. Lovell, "On the Spacing Between Aggregate Grains in Concrete and the Dimension of the Aureole de Transition," pp. C42 in *Liaisons Pates De Ciment Materiaux Associes*. RILEM, Toulouse, France, 1982.

[62]E.J. Garboczi and D.P. Bentz, "Computational Materials Science of Cement-Based Materials," *MRS Bull.*, **28** [3] 50–4 (1993).

[63]E.J. Garboczi and D.P. Bentz, "Computer Simulation of the Diffusivity of Cement-Based Materials," *J. Mater. Sci.*, **27**, 2083–92 (1992).

[64]X. Ping, J.J. Beaudoin, and R. Brousseau, "Flat Aggregate-Portland Cement Paste Interfaces, I. Electrical Conductivity Models," *Cem. Concr. Res.*, **21**, 512–22 (1991).

[65]X. Ping, J.J. Beaudoin, and R. Brousseau, "Flat Aggregate-Portland Cement Paste Interfaces, II. Transition Zone Formation," *Cem. Concr. Res.*, **21**, 718–26 (1991).

[66]D. Bretton, J.P. Ollivier, and G. Ballivy, "Diffusivite des Ions Chlore dans la Zone de Transition entre Pate Ciment et Roche Granite"; pp. 269–78 in *Interfaces in Cementitious Composites*. Edited by J.C. Maso. E & FN Spon, London, 1992.

[67]U. Costa, M. Facoetti, and F. Massazza, "Permeability of the Cement-Aggregate Interface: Influence of the Type of Cement, Water/Cement Ratio, and Superplasticizer"; pp. 392–401 in *Admixtures for Concrete: Improvement of Properties*. Edited by E. Vazquez.

[68]Y.F. Houst, H. Sadouki, and F.H. Wittmann, "Influence of Aggregate Concentration on the Diffusion of CO_2 and O_2"; pp. 279–88 in *Interfaces in Cementitious Composites*. Edited by J.C. Maso. E & FN Spon, London, 1992.

[69]X. Ping and T. Ming-shu, "Effect of Portland Cement Paste-Aggregate Interface on Electrical Conductivity and Chemical Corrosion Resistance of Mortar," *Il Cemento*, **85** [1] 33–42 (1988).

[70]P.B. Bamforth, "The Water Permeability of Concrete and Its Relationship with Strength," *Mag. Concr. Res.*, **43** [157] 233–41 (1991).

[71]M.H. Zhang and O.E. Gjorv, "Permeability of High-Strength Lightweight Concrete," *ACI Mater. J.*, **88** [5] 463–9 (1991).

[72]R.D. Cook, D.S. Malkus, and M.E. Plesha, *Concepts and Applications of Finite Element Analysis*. John Wiley and Sons, New York, 1989.

[73]A.R. Day and E.J. Garboczi, "DC Conductivity and Elastic Moduli of a Model Interpenetrating Phase Composite," unpublished work.

[74]F. Holuj, M. Drozdowski, and M. Czajkowski, "Brillouin Spectrum of $Ca(OH)_2$," *Solid State Commun.*, **56**, 1019–21 (1985).

[75]F.H. Wittman, "Estimation of the Modulus of Elasticity of Calcium Hydroxide," *Cem. Concr. Res.*, **16**, 971–2 (1986).

[76]E.J. Garboczi and A.R. Day, "Computer Simulation Computation of the Elastic Moduli of C_3S Cement Paste," unpublished work.

[77]T.Y. Lyubimova and E.R. Pinus, "Crystallization Structure in the Contact Zone Between Aggregate and Cement in Concrete," *Colloid J. (USSR)*, **24**, 491–8 (1962).

[78]S. Wei, J.A. Mandel, and S. Said, "Study of the Interface Strength in Steel Fiber-Reinforced Cement-Based Composites," *ACI J.*, **83**, 597–605 (1986).

[79]J.A. Larbi, and J.M.J.M. Bijen, "Orientation of Portlandite at the Paste-Aggregate Interface and Strength Development of the Paste-Aggregate Bond in Mortars in the Presence of Microsilica"; pp. 271–85 in *Ceramic Transactions, Volume 16: Advances in Cementitious Materials*. Edited by Sidney Mindess. The American Ceramic Society, Westerville, OH, 1991.

[80]M. Kawamura, and S. Igarashi, "Fracture Toughness for Steel Fiber-Cement Paste Interfacial Zone," *J. Mater. Civil Eng.*, **4**, 227–39 (1992).

[81]Q. Yun and C. Qingli, "Studies of the Interfacial Bond Between Cement Pastes and Expanded Shale"; pp. 71–7 in *Interfaces in Cementitious Composites*. Edited by J.C. Maso. E & FN Spon, London, 1992.

[82]U. Schneider and S. Chen, "The Interface Zone Around Expanded Shale Grain in Hardened Cement Paste"; pp. 149–56 in *Interfaces in Cementitious Composites*. Edited by J.C. Maso. E & FN Spon, London, 1992.

[83]J.N. Plendl and P.J. Gielisse, "Hardness of Nonmetallic Solids on an Atomic Basis," *Phys. Rev.*, **125**, 828–32 (1962).

[84]T.T.C. Hsu, F.O. Slate, G.M. Sturman, and G. Winter, "Microcracking of Plain Concrete and the Shape of the Stress-Strain Curve," *J. ACI*, **2**, 209–24 (1963).

[85]E. Schlangen and J.G.M. Van Mier, "Experimental and Numerical Analysis of Micromechanisms of Fracture of Cement-Based Composites," *Cem. Concr. Composites*, **14**, 105–18 (1992).

[86]E. Schlangen, "Experimental and Numerical Analysis of Fracture Processes in Concrete"; Ph.D. Thesis, Delft University of Technology, Delft, The Netherlands, 1993.

[87]E. Schlangen and J.G.M. Van Mier, "Micromechanical Analysis of Fracture of Concrete," *Int. J. Damage Mech.*, **1**, 435–54 (1992).

[88]E. Schlangen and J.G.M. Van Mier, "Simple Lattice Model for Numerical Simulations of Fracture of Concrete Materials and Structures," *Mater. Struct.*, **25**, 534–42 (1992).

[89]E. Schlangen and J.G.M. Van Mier, "Fracture Modelling of Granular Materials"; pp. 153–8 in *Computational Methods in Materials Science*, MRS Symposium Proceedings, Vol. 278. Edited by J.E. Mark, M.E. Glicksman, and S.P. Marsh. Materials Research Society, Pittsburgh, 1992.

[90]A.H.J.M. Vervuurt, E. Schlangen, and J.G.M. Van Mier, "Pull-out of Steel Anchors Embedded in Concrete"; pp. 569–78 in *Special Seminar on Anchorage Engineering*. Chapman and Hall, London, 1993.

[91]E. Schlangen and J.G.M. Van Mier, "Numerical Study of the Influence of Interfacial Properties on the Mechanical Behaviour of Cement-Based Composites"; pp. 237–46 in *Interfaces in Cementitious Composites*. Edited by J.C. Maso. E & FN Spon, London, 1992.

[92]H.J. Herrmann, H. Hansen, and S. Roux, "Fracture of Disordered, Elastic Lattices in Two Dimensions," *Phys. Rev. B*, **39** [1] 637–48 (1989).

[93]R. De Borst, G.M.A. Kusters, P. Nauta, and F.C. De Witte, "DIANA—A Comprehensive but Flexible Finite Element System"; in *Finite Element Systems Handbook*, 3rd Edition. Springer-Verlag, Berlin, 1986.

[94]Z.P. Bazant, M.R. Tabbara, M.T. Kazemi, and G. Pijaudier-Cabot, "Random Particle Model for Fracture of Aggregate or Fiber Composites," *J. Eng. Mech., ASCE*, **116** [8] 1686–705 (1990).

[95]A. Berg and U. Svensson, "Datorsimulering och analys av brottforlopp i en heterogen material struktur." Report No. TVSM-5050, Lund Institute of Technology, Division of Structural Mechanics, Lund, Sweden, 1991.

[96]N.J. Burt and J.W. Dougill, "Progressive Failure in a Model Heterogeneous Medium," *J. Eng. Mech. ASCE*, **103** [3] 365–76 (1977).

[97]E. Schlangen and J.G.M. Van Mier, "Fracture Simulations in Concrete and Rock Using a Random Lattice"; pp. 1641–6 in *Computer Methods and Advances in Geomechanics*. Edited by H.J. Siriwardane and M.M. Zaman. Balkema, Rotterdam, 1994.

[98]P.E. Roelfstra, H. Sadouki, and F.H. Wittman, "Le Beton Numerique," *Mater. Struct.*, **18**, 327–35 (1985).

[99]J.C. Walraven, J.C., "Aggregate Interlock: A Theoretical and Experimental Analysis"; Ph.D. Thesis, Delft University of Technology, Delft, The Netherlands, 1980.

[100]J.G.M. Van Mier, "Fracture Process Zone in Concrete: A Three-Dimensional Growth Process"; pp. 567–72 in *Fracture Behaviour and Design of Materials and Structures*. Edited by D. Firrao. EMAS Publishers, Warley, 1990.

[101]J.G.M. Van Mier, "Mode I Fracture of Concrete: Discontinuous Crack Growth and Crack Interface Grain Bridging," *Cem. Concr. Res.*, **21**, 1–15 (1991).

[102]Z.P. Bazant and P.A. Pfeiffer, "Shear Fracture Test of Concrete," *Mater. Struct. (RILEM)*, **110** [19] 111–21 (1981).

[103]S. Mindess, "Interfaces in Concrete"; pp. 163–80 in *Materials Science of Concrete I*. Edited by J.P. Skalny. The American Ceramic Society, Westerville, OH, 1989.

[104]J. Baron, A. Bascoul, G. Escadeillas, and G. Chaudouard, "From Clinker to Concrete—An Overall Modelling," *Mater. Struct.*, **26**, 319–27 (1993).